UNCLASSIFIED

AD NUMBER

AD355863

CLASSIFICATION CHANGES

TO: unclassified

FROM: confidential

LIMITATION CHANGES

TO:

Approved for public release, distribution unlimited

FROM:

AUTHORITY

OCA; 12 Aug 1975 IAW document markings; AFWL Notice 31 Oct 1975

THIS PAGE IS UNCLASSIFIED

AD 355863L

DEFENSE DOCUMENTATION CENTER

FOR

SCIENTIFIC AND TECHNICAL INFORMATION

CAMERON STATION ALEXANDRIA. VIRGINIA

GENERAL ATOMIC DIVISION
GENERAL DYNAMICS CORPORATION

John Jay Hopkins Laboratory for Pure and Applied Science
P.O. Box 608, San Diego 12, California

GAMD-4468
Category A

This document consists of 97 pages.
No. __ of 25 copies, Series A.

THERMAL PHENOMENA IN THE FIREBALL (U)

Further distribution of this document outside the
Department of Defense or the U. S. Atomic Energy
Commission, or its reproduction in whole or in part
or summarizing or microcarding is prohibited without
prior written approval of the Contracting Officer,
Air Force Special Weapons Center, Kirtland Air Force
Base, New Mexico.

Work done by:

B. E. Freeman
D. E. Harris
W. B. Lindley
R. W. Paul
M. L. Young

DOWNGRADED AT 3 YEAR INTERVALS
DECLASSIFIED AFTER 12 YEARS

Report written by

B. E. Freeman

This document, which was prepared primarily for
internal use at General Atomic, may contain
preliminary or incomplete data. It is informal
and is subject to revision or correction; it
does not, therefore, represent a final paper.

Air Force Special Weapons Center
Contract AF29(601)-6105

Project No. 357
August 12, 1963

TABLE OF CONTENTS

LIST OF ILLUSTRATIONS

ABSTRACT

Results of three calculations of the impulsive interaction of thermal radiation from high-altitude nuclear explosions with targets within the fireball (the thermomechanical effect) are reported. These problems constitute a preliminary investigation into techniques of calculation and phenomena of importance to be followed later by a survey to establish lethal radius envelopes. The interaction with 200-KT yield at 60,000-ft altitude is found to be predominantly the effect of the blast wave which is perhaps just lethal at a range of 2.5×10^4 cm. The interaction of the same yield at 90,000 ft, however, does show important thermomechanical as well as blast effects. The lethal radius is found to be greater than 3.0×10^4 cm. Presentation of the calculated results is supplemented by discussion of the method of calculation, preparation of initial data, and evaluation of assumptions constituting the interaction model.

INTRODUCTION

Preliminary results of calculations of the interaction of thermal radiation from a nuclear explosion with an object within the fireball are presented. The effect, called the thermomechanical effect (TME), results from the irradiation of a structure by intense thermal energy emitted by the heated air and the subsequent vaporization and blowoff of the heated vapor. The reaction of the blowoff to exert an impulse on the structure produces the TME.

In this report three calculations are described in some detail. Two of these use the environment created by a 200-KT yield at 90,000-ft altitude and differ in the range of the object (called for convenience a re-entry vehicle, or R.V.) from the origin of the explosion. These ranges are: problem 1, 2.5×10^4 cm, and problem 2, 3.0×10^4 cm. The third problem represents interaction with an R.V. at range 2.5×10^4 cm from a 200-KT explosion at 60,000 ft.

Material in the report is organized into three sections. In Section I a current statement of characteristics of the General Atomic interaction code, SUPER SPUTTER, is presented. This code has been used to perform the TME calculations presented here as well as to investigate other interaction phenomena. Section II contains an analysis of the explosion environment to obtain boundary conditions for the TME calculations. A critique is also presented of some of the assumptions made about the environment. Finally, in Section III the calculations are analyzed in some detail to present the characteristics of the TME interaction process.

At 60,000-ft altitude it is found that the effect of ambient fireball pressure is much more important than ablation pressure in determining the impulsive loading. Consequently, this altitude is below the altitude where the TME plays a role and is properly considered in the blast regime. At 90,000 ft both ambient and ablation pressures are important. This is a transition region between effects. The lethal range appears to be greater

than 3×10^4 cm. An interesting and important effect of abrupt heating and ionization of the R.V. vapor is identified in the problems at 90,000 ft. Its quantitative description may depend sensitively on low-temperature radiative properties.

While calculations presented here by no means constitute an exhaustive survey of the TME, it is thought that presentation of early results will accomplish the following results:

1. Acquaint a wider audience with techniques available for application to the TME and similar problems.

2. Document more currently and in greater detail the calculational methods and material properties in use.

3. Prompt criticism of the approach to the calculation of the TME.

Additional calculations are now planned to detail the lethal radius as a function of altitude. Further improvements in code and environment specification are also being incorporated.

I. THE SUPER SPUTTER CODE

Calculations of the TME have used SUPER SPUTTER, a general purpose, one-dimensional radiation transport hydrodynamics code based on the Lagrangian description of the fluid. Several modifications of this code have been made to carry out TME calculations. In the following sections the most important of these code changes are described in order to illuminate the nature of the physical model and some of the mathematical approximations being used.

In section A the photon source treatment is described in complete detail; section B indicates how the ambient pressure inside the fireball is applied as a boundary condition to the vapor; section C describes the treatment of transition between vapor and solid at the "boiling" interface and the divergence of expanding vapor; section D indicates how deviations from local thermodynamic equilibrium which may occur in optically thin and low-density regions are taken into account; section E describes the radiation transport routine used in the code; section F gives a brief description of newly incorporated features of the problem generator code which, in addition to preparing initial data, allows redistribution of zones during the course of the problem. Finally, section G describes the properties assumed for the target material and presents previously unpublished calculations for some of the temperature-density regime.

The successful completion of a number of problems described below has both tested the modifications mentioned herein as well as shown up some inconsistency in the angular distribution used in an earlier calculation.[1] The new routines have been thoroughly checked and are producing consistent results with obvious improvements. In one case a comparison of two runs differing in the angular distribution of the source which resulted from an earlier incorrect source formulation is presented. The error, contained in our first report[2] on the thermomechanical source, has been corrected in the description of the first section and does not occur in the remainder of problem results presented.

A more complete report on the SUPER SPUTTER code is now in preparation, with publication expected shortly.

A. THERMAL SOURCE

The SUPER SPUTTER code will be used to calculate the interaction of a high-temperature radiative source on an object placed within the thermal environment. The description of the problem is most closely approximated by that for the single-frequency source used in the investigation of optical interactions.[3]

A generalization of the optical-interaction source has been made to describe the thermal interaction. In it the incident radiation is assumed to fall on the locally plane surface of the target or target vapor. The source is characterized by a total intensity which may change with time, a frequency distribution approximated by representative groups of photons, and one of several different choices of angular distribution. The photon groups are absorbed in the target vapor according to an approximation to the ionic absorption coefficient which takes into account free-free and bound-free transitions of the ionized vapor. This coefficient depends on the photon frequency ν, the material temperature Θ, and density ρ, as well as on the target material and degree of ionization. The absorption of each frequency group in the vapor is determined by numerical integration to find the optical depth from the surface corrected for induced emission at the frequency in question. The flux is then obtained as a function of the optical depth and parameters specifying the nature of the incident angular distribution.

The Source

The thermal source is specified by the angular and frequency distributions of the photons incident on the target. While in the most general problem these distributions cannot be factored and depend on the time, in this first approach several simplifying assumptions have been made. Perhaps most fundamental of these is that the frequency and angular distributions may be factored into a product of two individual distributions, one of which depends only on frequency and the other only on angle.

Angular Distribution

The source routine now offers three options for the photon angular distribution, each of which is a simple, time-independent function for which angular groups are unnecessary. The choices are:

1. Isotropic distribution, $I(\Omega) = I_o$.
2. Cos distribution, $I(\Omega) = I_o\mu$.
3. Ray or pencil distribution, $I(\Omega) = I_o\delta(\bar{\Omega} - \bar{\Omega}_o)$

In the second distribution μ is the cosine of the angle from the ray direction to the normal to the assumed plane target. In the last distribution a pencil of photons falls on the target in the $\bar{\Omega}_o$ direction for which $\mu = \mu_o$. All of these distributions allow the planarity of the interaction to be preserved and lead to the following simple functions $f(x)$ describing the net flux, $\emptyset = \int(\Omega) \cos \Theta \, d\Omega$, of the source photons at optical depth x normal to surface within the target:

1. $f(x) = 2E_3(x)$
2. $f(x) = 3E_4(x)$
3. $f(x) = \mu_o \exp(-x/\mu_o)$

Each of the distributions is normalized to 1 at x = 0 if the distribution is symmetrical about the normal. For case 3 and oblique incidence ($\mu_o \neq 1$), the coefficient μ_o takes into account the increased target area intercepted by a beam having unit area normal to the ray.

The first option is relevant to the thermal source inside an optically thick fireball where isotropy of the radiation obtains. Well outside the fireball radiation comes from a rather localized direction represented by the pencil of option 3. Option 2 is an intermediate case perhaps appropriate near the edge of the fireball.

Addition of further simple options is easily made. Angular grouping for a complex distribution, however, would present a harder but still tractable job.

Frequency Distribution

Photons in the incident beam are described by a distribution function $f(v)$ which is assumed to depend on time but not on angle. The source calculation approximates this distribution in the frequency group approximation wherein the photons falling within the interval (v_n, v_{n+1}) according to the absorption coefficient of a representative frequency. In the general case the intensities A_n within these groups would be permitted to depend on time in a quite arbitrary way as, for example, when specified by piece-wise linear expressions.

In the special case of the black body function, $f(v) = \dfrac{B_v}{\int_0^\infty B_v \, dv}$, the frequencies may be chosen in such a way that considerable simplification results through maintaining a constant time-independent ratio between groups even though the black body source temperature Θ_0 may change with time. This is accomplished by the assignment $v_n = u_n \Theta_0 / h$ in which the u_n are constants chosen to give the desired accuracy in the source description. The frequency group boundaries, consequently, depend on time through time-dependence of Θ_0. A representative choice of frequency groups and weights for a black body is given in Table 1. The A_n are normalized to give unit sum.

Table 1. Nine-group Constants

n	Group Boundary $h v / \Theta_0$	An	Average Energy $E_n = h v / \Theta_0$
	0		
1	1.0	0.05	0.5
2	2.0	0.14	1.5
3	3.0	0.21	2.5
4	4.0	0.20	3.5
5	5.0	0.16	4.5
6	6.0	0.10	5.5
7	8.0	0.10	7.0
8	10.0	0.03	9.0
9	12.0	0.01	11.0

In the currently available version of the source the group constants are loaded into the code from Table 1 for application to the black body source. The black body intensity, $\sigma \Theta_0^4$, is allowed to change with time through specification of constants in a piece-wise linear variation of Θ_0 with time. Generalization of the routine to calculate non-black body cases is made trivially if the intensity is independent of time and requires additional coding to provide the description of the time dependence of the intensities for the more general problem.

Source Energy Deposition

The amount of energy q_i [ergs/(cm^{2}sec)] deposited in each of the zones of the vapor is bounded by Lagrangian coordinates x_i and x_{i+1}. The source is obtained by taking the difference between the net fluxes ϕ_i incident on and emergent from the zone in question.

$$q_i = \phi_i - \phi_{i+1}$$

The flux is formed from the finite difference approximation to the following expression for the total net flux integrated over frequency and angles:

$$\phi(x) = \dot{E} \int_0^\infty f(x_\upsilon) f(\upsilon) d\upsilon$$

where $\dot{E}$ is the integrated intensity falling on the target and x_υ is the optical depth at frequency υ measured normal to the target surface $x_\upsilon = \int_0^x \rho K_\upsilon(x') dx'$. In the finite difference approximation for the frequency groups and zones, this becomes $\phi_i = \dot{E} \sum_n A_n f_j(x_n)$, where x_n is the optical depth for the nth group and f_j can take the form of the three options given above.

For the black body source

$$\phi_i = 2\dot{E}f\sum_n A_n E_3 [\int_0^{x_i} K_n(x)\rho dx$$

where the optical depth is approximated

$$\int_0^{x_i} K_n(x)\rho dx = \sum_{j=1}^{i-1} \rho_j K(\upsilon_n, \Theta_j, \upsilon_j) \cdot (x_{j+1} - x_j),$$

$\dot{E} = \sigma\Theta_0^4$, and f is a constant to allow for $1/r^2$ reduction in intensity.

Flow Diagram

The specification given above has been incorporated into the "QUE" subroutine. This routine, one among several options which may be incorporated into SPUTTER, is selected for thermal mechanical effect calculations while other subroutines remain largely in standard form. The logical flow of the

code subroutine is given in Appendix A of this report, together with the
FORTRAN instructions corresponding to it. Both flow diagram and code apply
to the black body source. Addition of a specification of the way in which
the frequency distribution changes with time will be required for the more
general frequency-dependent problem.

Vapor Absorption Coefficient

The Raĭzer approximation to ionic absorption coefficient[4,5] is used
to obtain the dependence on frequency, material temperature, density and
species. The prescription including induced emission is

$$K_\nu = \begin{cases} K_{ff}(e^u - 1) & \text{if} \quad u < u_K \\[2ex] K_{ff}(1 - e^{-u})e^{u_K} & \text{if} \quad u \geq u_K \end{cases}$$

where

$$K_{ff} = 8.62 \times 10^{10} \frac{Z \, \bar{Z} \, \rho}{A^2 (h\nu)^3 \Theta^{\frac{3}{2}}}$$

and

$$u_K = \min(u_1, \ell n_e \Gamma)$$

$$u_1 = K\text{-shell energy} = \frac{13.6 \, Z^2}{\Theta}$$

$$\Gamma = \text{electron degeneracy parameter} = \frac{10^{-2} A \Theta^{3/2}}{\rho \, Z}$$

Other quantities appearing are

A = atomic number of target material

ρ = density (gm/cm^3)

Θ = temperature (ev)

$h\nu$ = photon energy (ev)

Z = mean number of free electrons per target atom (obtained in the equation of state subroutine)

$u = h\nu/\Theta$

$$\bar{Z^2} = \begin{cases} Z & \text{if} \quad Z < 1 \\[1ex] Z^2 & \text{if} \quad Z \geq 1 \end{cases} \quad \text{Mean square number of free electrons}$$

Future Applications

Further generalization and improvement of the interaction code would indicate modification in at least two respects:

1. A more general angular distribution would require analysis to determine how the angular integrals may be performed. It is likely that a simple distribution could be handled analytically while a more complicated one would require angular grouping.

2. Optical properties in the ionic region exist for some target materials in greater detail than the Raizer approximation. For these (e.g., CH_2, air, Be, Si, Al) the deposition can be more accurately performed in principle. In practice, however, this treatment contains many of the limitations of the many-frequency radiation transport, primarily in lengthy, slow calculation. It is probable that improved material properties can be used in the source without excessive lengthening of the code. The low temperature material properties (solid and molecular regimes) are known very poorly, constituting a limitation for applications having small incident radiant flux. Additional work is needed for this use as well as for the optical interaction application at low incident power.

B. PRESSURE BOUNDARY CONDITION

Air inside the fireball heated to its ambient temperature exerts a pressure which, increasingly at lower altitudes, influences the hydrodynamics of the vapor blowoff. When the air pressure is comparable with or exceeds the ablation pressure, $\dot{m}c$, the blowoff is inhibited, the density remains high, and vapor opacity is affected. This pressure also increases the impulse experienced by the target. If the velocities of the air and vapor remain small compared with thermal velocities, the effect of the air is to apply a static pressure to the air-vapor interface, constituting a boundary condition. Further discussion of this point is found in section II.D. At a particular radial distance from the explosion point this pressure, given by the ambient fireball pressure, changes with time as shown typically in Fig. II.2.

Modification of the SUPER SPUTTER code has been made in the HYDRO subroutine to accommodate the externally applied boundary pressure. The

boundary condition at the vapor-air interface is given in the form of a piece-wise linear fit in time to the ambient fireball temperature. Flow diagram and code are presented in Appendix B.

C. BOILING AND VAPOR DIVERGENCE

In order to describe the transition from solid to vapor, called "boiling," it is assumed that a "boiling" temperature, Θ_b, and a constant specific heat, C_V, can be defined for the solid. In turn a specific energy for "boiling", $H_C = C_V\Theta_b$, is then known. When an element of mass is heated to Θ_b, it is assumed that an additional amount of specific energy H_V, called the vaporization energy, is required before the vaporization will occur and the temperature can change. For $E > H_C + H_V$, the material is described in terms of vapor equations of state.

As vapor is evolved at the solid-vapor interface, it expands, dropping in density. If it continued to expand in only one direction, a steady state could not be achieved in the vapor. In fact the vapor will tend to expand parallel to the target surface also. In order to take this effect into account, a mass depletion scheme has been added to the code.

The radial divergence can be approximately taken into account in a Lagrangian plane geometry calculation if the mass in a given zone is reduced as the zone expands. A parameter $\bar{r}$, the radius of the target or target area in the case of a laboratory experiment, is introduced into the calculation. The mass of a given zone on each time cycle is then said to be

$$m_\ell^{\,n} = \left\{ \frac{\bar{r}}{\bar{r} + c(z_\ell^{\,n} - z_\ell^{\,0})} \right\}^2$$

or

$$m_\ell^{\,n} = \left\{ \frac{r_\ell^{\,n-1}}{r_\ell^{\,n}} \right\}^2 m_\ell^{\,n-1} \quad,$$

where

$$r_\ell^{\,n} = \bar{r} + c(z_\ell^{\,n} - z_\ell^{\,0})$$

and $z_\ell^{\,n}$ is the average position, measured perpendicularly to the target surface at time zero, of the zone ℓ at time n. This treatment assumes that:

(1) the vapor diverges parallel to the target surface at the same rate at which it expands perpendicularly to the surface; (2) the temperature and density of the material are functions of z and t only; and (3) vapor which flows out of a tube perpendicular to the target surface and of radius $\bar{r}$ can be removed from the calculation and ignored. The work done and the total energy removed from the calculation as this material is removed from the zone is taken into account.

D. DEVIATIONS FROM LOCAL THERMODYNAMIC EQUILIBRIUM

In the very low density leading edge of the blownoff vapor, the material becomes optically thin. When this occurs the local equilibrium between the material and the radiation field is maintained only if the rate of increase of the internal energy by collisional ionization ($\dot{E}_{col}$) exceeds the rate of decrease by radiation recombination ($\dot{E}_{rec}$). This breakdown of the local equilibrium between the radiation field and the material will, in general, occur before the random kinetic energy of the ions and electrons fall out of local equilibrium with one another. If it is assumed that the ions and electrons are in equilibrium, then separate rate equations for the internal energy due to random kinetic energy of the ions and electrons (R) and the internal energy due to ionization and excitation (I) can be integrated if the material is described in terms of three independent variables: temperature, density, and the mean number of free electrons per average ion ($\bar{Z}$). The correct radiation rate can be expressed in terms of Θ, ρ, and $\bar{Z}$ also. In order to do this, I as a function of $\bar{Z}$ for the material in question must be known. In the numerical calculation, LTE is assumed in a mass element until the material is optically thin and $\dot{E}_{rec} \geq \dot{E}_{col}$. From that point on, $\dot{E}_{col}$ is ignored and separate equations for $\dot{R}$ and $\dot{I}$ are integrated in terms of ρ, Θ, and $\bar{Z}$. The radiation rate due to recombination and bremsstrahlung is calculated, and the absorption of energy due to self-radiation is ignored. This correction in general reduces the amount of energy radiated out of the vapor.

E. RADIATION TRANSPORT

The radiation transport subroutine FLASH,[6] used in plane geometry interaction calculations, has been recoded to make more accurate and faster use of the exponential integrals. This routine has also been coupled with a diffusion calculation for optically thick zones in order to speed up the calculation, in particular, for the multifrequency time-dependent code expected to be operational soon. The present multifrequency code does a "snapshot" calculation using group absorption coefficients stored on magnetic tape.

The multifrequency calculation brings into core storage a single frequency at a time. This calculation is repeated until all groups have been processed. The calculation will be performed as a part of the regular SUPER SPUTTER cycle to perform a truly frequency-dependent calculation; however, in practice the calculation is at present too slow to do more than a few successive cycles for a test. These snapshot calculations are used primarily to evaluate radiative properties of the system and to compare with (and hopefully correct) the mean absorption coefficient results used in the time-dependent calculation.

F. PROBLEM GENERATOR CODE AND REZONE

1. SUPER SPUTTER Variables for Generating and Rezone

R_i = distance in centimeters from the origin

$DELTAR_i$ = $R_{i+1} - R_i$

G_i = mass in grams at $i + \frac{1}{2}$ (for sphere is G_i = (zone mass)/($\frac{4\pi}{3}$))

$THETA_i$ = temperature in electron volts at $i + \frac{1}{2}$

RD_i = velocity in cm/sec of R

SV_i = specific volume at $i + \frac{1}{2}$ in cm/gm (plane) or cm^3/gm (sphere)

A_i = cross sectional area at i in cm^2

ASQ_i = A_i^2

P_i = (material + radiation + viscous) total pressure at $i + \frac{1}{2}$ in ergs/cm or ergs/cm^3

E_i = specific internal energy from equation of state at $i + \frac{1}{2}$ in ergs/gm

EI_i = specific internal energy from integration at $i + \frac{1}{2}$ in ergs/gm

$SMLR_i$ = radius of depleted mass

IMDA = zone of constant material properties.

2. Generating

The above variables are generated for slab or spherical geometry. Options of zoning by mass or by radius are available. In each case a constant, σ, is specified giving the ratio of either mass or radius increment to the corresponding quantity for neighboring zones. This quantity is constant within a region but has possibly different values in different regions. Combinations of the quantities of a number of zones, interface mass or DELTAR, may be specified to complete the problem setup. Among these the possibility of matching G or DELTAR across IMDA interfaces exists.

The flow of the solution is:

(1) Input cards are read which describe the density, temperature and velocity at several discrete positions in the system. Then the coefficients of a segmented function fit (constant through cubic) are calculated for the density profile, THETA profile, and RD profile.

(2) An input IMDA zone card is read which establishes for the IMDA zone: (a) the left and right limits (cm), (b) a description of how mass points are to be generated, and (c) material constants. Then 3, 4 and 5 below are executed, finally followed by editing and initiation of calculation.

(3) Whether generating or rezoning, given the left and right boundaries (cm) there are six quantities available to describe how the generated mass points shall be related to each other. Any two of the following (a)-(d) constitute a complete prescription, and are a means of describing what the ratio of G_{i+1}/G_i shall be. (a) The mass of the leftmost mass point, (a1) or the length of the leftmost mass point; (b) the mass of the rightmost mass point, (b1) or the length of the rightmost mass point, (c) the constant ratio of G_{i+1}/G_i, (d) the number of mass points to generate. To equate (a) or (a1) with the unknown previous last mass point gives only one of the specifications (b), (b1), (c), or (d). Special: if the prescription if (a1), (b1), or just (b1), the ratio of the mass points is then by DELTAR rather than their G. G_i, $DELTAR_i$, and R_i are calculated.

(4) $THETA_i$ are interpolated from the THETA profile.

(5) RD_i are interpolated from the RD profile.

(6) SV_i, A_i, ASQ_i are calculated.

(7) E_i, EI_i, P_i are calculated.

(8) $SMLR_i$ (for mass depletion) are transferred from an input storage array.

3. Rezoning

The rezoning process first establishes a step function density profile for the problem to be rezoned. A linear segmented fit is calculated for the RD profile, and another for the SMLR profile if there is mass depletion.

Rezone input cards are read and facilities are considered for: deleting or adding mass; continuing or rezoning old mass points; prescription for how to rezone old mass points or generate new mass points; whether to delete, add, alter, or preserve LMDA interfaces; whether to add a pusher. (3) above is utilized for rezoning and adding mass points and RD and SMLR are interpolated from their profiles. Unchanged mass points retain their original values of the variables.

When rezone input is exhausted, (6) is employed. Rezoned mass points have a calculation of $THETA_i$ (conserving old internal energy). New mass points get their $THETA_i$ from rezone input. E_i, EI_i, P_i are calculated for new and rezoned mass points.

G. MATERIAL PROPERTIES

Calculations of the TME presented herein required thermodynamic and optical properties for the target material properties for the target material. The properties for polyethylene with composition $(CH_2)_n$ as representative of an ablative material having low thermal conductivity and large specific heat have been used. Two regimes are to be distinguished: that in which the temperature is low and ionization is small, and the ionic region at higher temperature.

In the low temperature region a simplified molecular equation of state is used. Below the vaporization temperature of 0.125 ev an average specific heat of 2.4×10^{11} ergs/(gm ev) applies. Thermal conductivity also is effective only in the solid where the conductivity is taken to be

10^{-3} cal/(cm sec $^{\circ}$K). The heat of vaporization is the small value 1.26×10^{11} ergs/gm, sufficient to depolymerize the plastic into C_2H_4. With subsequent heating dissociation into atomic C and H occurs in an abrupt but continuous transition whose transition temperature depends weakly on the density, with a value of ~ 0.4 ev for the problems of interest. A dissociation energy of 8.5×10^{11} ergs/gm is used. Optical properties in the region below 1 ev are based on extrapolation from calculations relevant to air, not taking into account the molecules and molecular ions actually present in CH_2 at temperatures below 1 ev. Correspondingly schematic representations of the Rosseland and Planck mean opacities are used. Further work is needed to remedy this deficiency for quantitative calculations on CH_2. It should be emphasized that the particular material composition is much more critical in this low temperature region than in the ionic regime at higher temperature.

In the ionic region the thermodynamic and optical properties have been calculated by the ionic model.[7] Results of unpublished calculations for CH_2 using the DIAPHANOUS code[8] have been incorporated into SPUTTER. Taking into account the line contribution to the optical absorption coefficient, the results represent an accurate estimate of optical properties of CH_2 as contained in the Rosseland optical mean free path used in the diffusion regimes and the spectral absorption coefficient used in the multifrequency "snapshot" calculations described above. While the absorption coefficients have not yet been published, the thermodynamic properties and the mean optical properties as calculated in DIAPHANOUS are presented in the table of Appendix C.

II. EXPLOSION ENVIRONMENT OF THE TARGET

In this section we present the environmental conditions assumed for the evaluation of the TME. Calculations of the effects of explosions of the XW50Y2[9,10] at the altitudes of 60,000 ft and 90,000 ft provide histories of environmental quantities at all radii of interest. Using these data, three calculations have been performed for the following altitudes of explosion h, and radii or target from explosion center, r.

Problem 1. $h = 90,000$ ft, $r = 2.5 \times 10^4$ cm.

Problem 2. $h = 90,000$ ft, $r = 3.0 \times 10^4$ cm.

Problem 3. $h = 60,000$ ft, $r = 2.5 \times 10^4$ cm.

We have assumed throughout the histories of the interaction that the relevant environmental quantities are the fireball local static pressure and isotropic black body thermal flux. We present these quantities in Section IIA for the three cases. In Sections B and C we examine, first, the validity of the black body assumption and, second, the arguments for neglecting effects associated with motion of air or target.

A. AMBIENT TEMPERATURE AND PRESSURE

In Fig. II-1 we show temperature vs time and in Fig. II-2 pressure vs time at the fixed radial distances corresponding to the three cases described above. These quantities are obtained as the result of some interpretation of quantities interpolated in position and plotted in time from the cited explosion calculations.

The structure exhibited by the temperature curves is interpreted as representing two phenomena in the explosion. At the distances chosen, a sharply defined shock has formed in the air and represents the first disturbance reaching the point in question. Associated with it is a rise in temperature corresponding to the material state resulting from the strong shock having a particular shock speed. While a slight temperature rise may occur in the material behind the shock, the rise is slight compared with the rather abrupt rise associated with the transit of the radiative front. This disturbance moves forward primarily by convection of the shocked air and

TEMPERATURE VS TIME AT SEVERAL POSITIONS
INSIDE THE FIREBALL

1. 2.5×10^4 CM, 90,000 FT
2. 3.0×10^4 CM, 90,000 FT
3. 2.5×10^4 CM, 60,000 FT

Fig. II-1

19

PRESSURE VS TIME AT SEVERAL POSITIONS
INSIDE THE FIREBALL

1. 2.5×10^4 CM, 90,000 FT
2. 3.0×10^4 CM, 90,000 FT
3. 2.5×10^4 CM, 60,000 FT
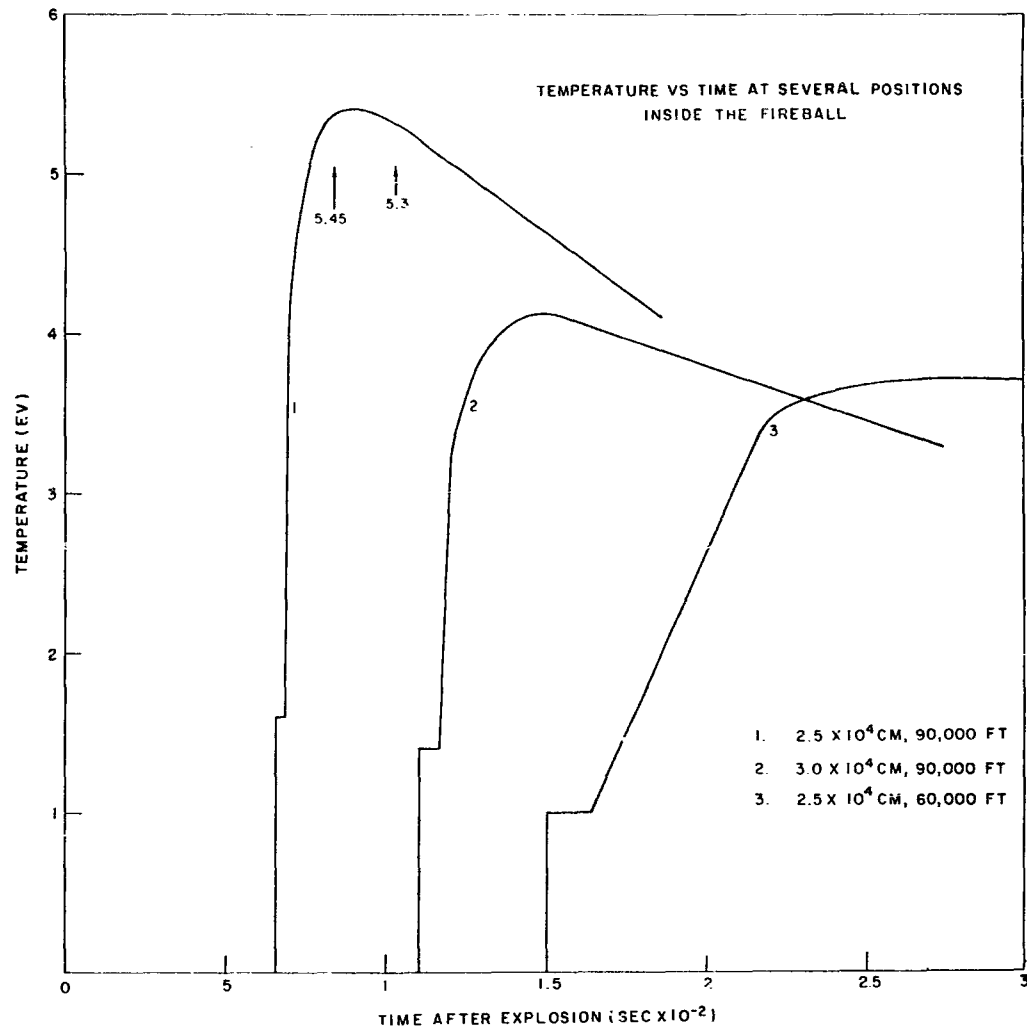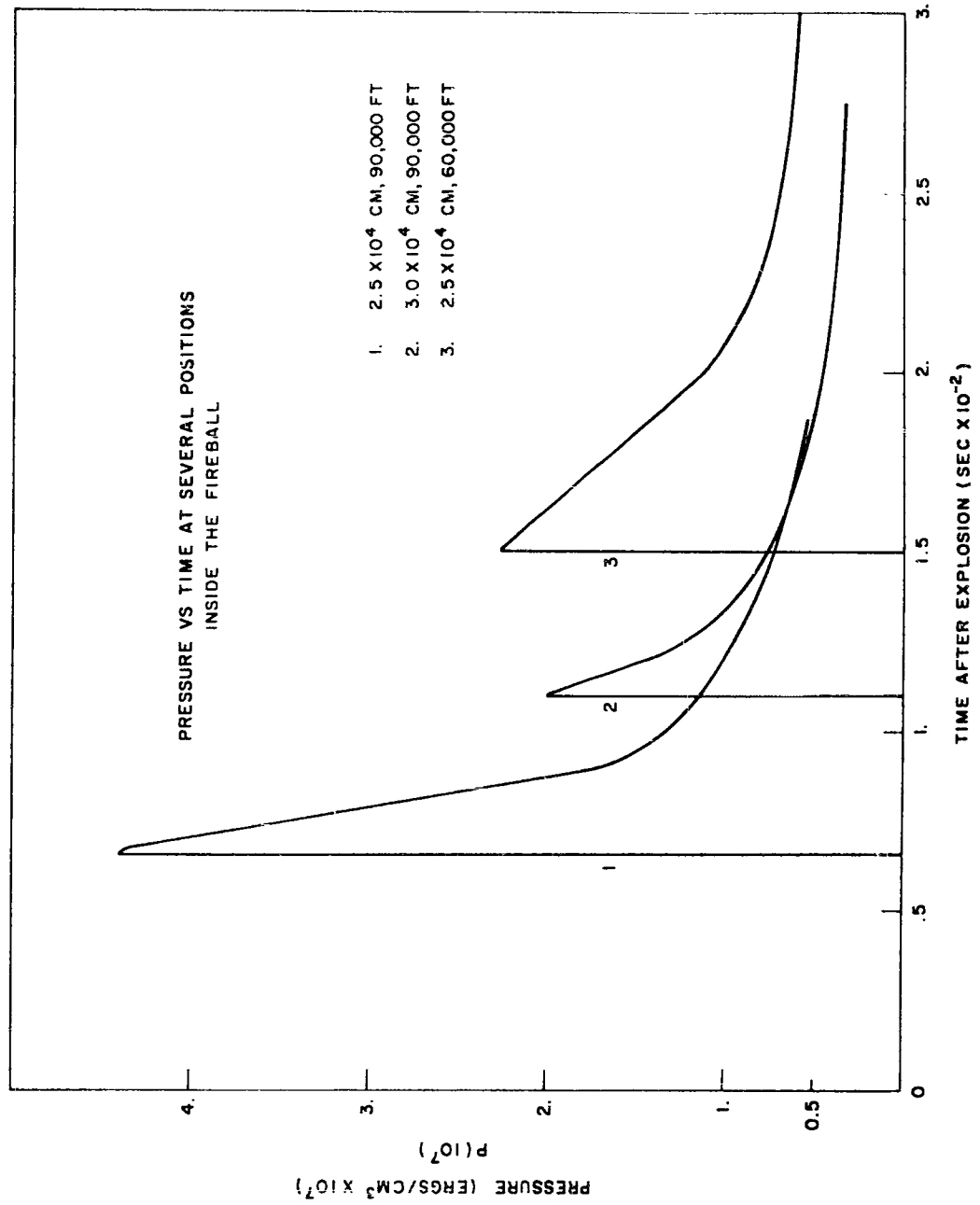
Fig. II-2

secondarily by diffusion of the front into additional cold material. The second rise leads rather quickly to the isothermal interior of the fireball which is seen to be considerably hotter than the shocked air. Since the radiative flux increases as the fourth power of temperature, it is seen that the second rise leads to fluxes almost two orders larger than in the shock.

Modifications of the explosion calculation data were found necessary to detail the duration of the shock plateau. Continuous mathematical rendering of the shock transition by the artificial viscosity leads, with limited numbers of zones, to washing out of the shock front. In each case, the shock front was identified and replaced in the curves by the more correct discontinuous profile. Duration of shock temperature was calculated by measuring plateau width and material velocity, a more accurate way than available with limited printouts in time. The very small preheating of air ahead of the shock by the emitted thermal flux was neglected, as was the flux itself before shock arrival.

B. RADIATIVE ENVIRONMENT

The calculations[9,10] of fireball early history used to obtain black body temperature also permit more detailed analysis to evaluate the validity of the black body assumption. At selected intervals during the explosion calculation frequency-dependent analysis calculations have been made determining the radiative flux and energy density throughout the fireball interior. Comparisons between the frequency-dependent radiation energy density and the corresponding black body quantity indicate the degree to which the black body distribution is justified. In Fig. III-3 these quantities are compared at several fireball radii 8.3×10^{-3} sec after explosion at h = 90,000 ft. While a complete analysis would call for the comparisons at successive times at the same position, qualitatively the same information is achieved by choosing positions (a) outside the shock front given in zone 53 corresponding to time just before the shock wave arrives, (b) inside the shock plateau given in zone 46 corresponding to the early shock heated history, (c) in the transition region in the radiative front given in zone 39 corresponding to the temperature rise from convection of the radiative front, and (d) in the isothermal sphere plateau given by zone 33 corresponding to the post temperature maximum period. One may conclude from Fig. III-3 that in general the
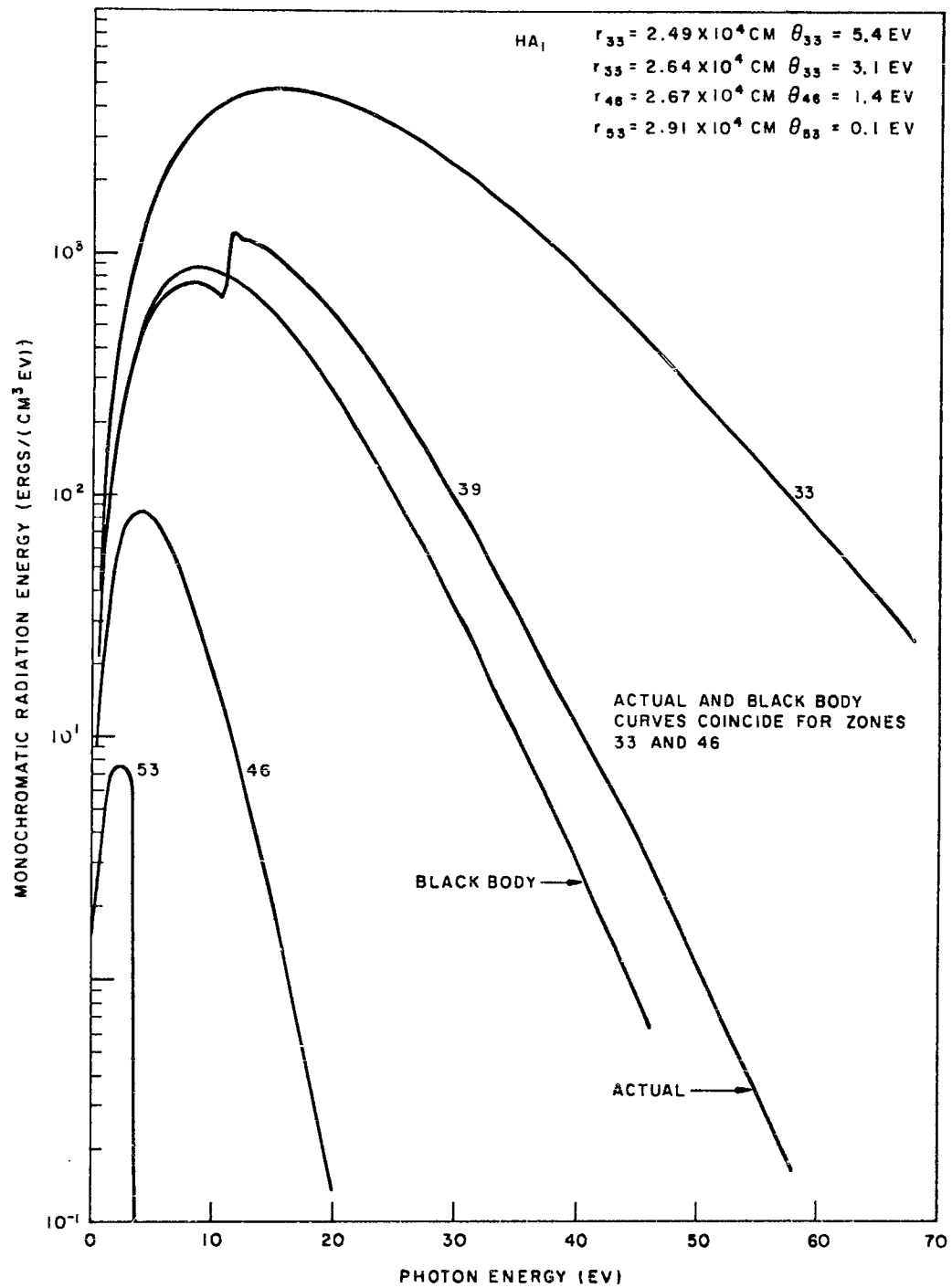
Fig. II-3--Source Energy vs Frequency

black body assumption is well justified. In the plateau regions, indeed, it is highly accurate, while in the transition region the occurrance of a photoelectric edge at ~ 11 ev introduces a small deviation which averages out in the black body curve. Ahead of the shock, of course, the radiation is highly nonthermal and anisotropic but with intensity which is not large enough, compared with the subsequent history, to be significant.

This conclusion is based on phenomena encountered at 90,000 ft and rather small target radii. While appreciably larger radii are not of interest at this altitude, interest in larger radii at higher altitudes suggests that the question be kept open. Indeed, the greater transparency of the fireball at higher altitudes indicates that deviations from thermality will be more important there.

Introduction of the target and its evolving vapor into the fireball will perturb to some degree the surrounding air by locally reducing the temperature. The assumption of thermal radiation at the unperturbed fireball temperature, consequently, is somewhat of an overestimate of the actual flux from the locally depleted air, Estimates have been made of the following effects which replenish the air cooled by the black body emission; first, the air may be heated again by radiative diffusion from more distant (but still nearby) unperturbed regions and second, undepleted air may be convected to the target by the streaming velocity induced by the shock wave.

Assuming that the local reduction in temperature is small, the radiative diffusion equation may be linearized so that the problem can be solved in closed form. The R.V. is assumed to be a perfectly absorbing sphere of radius a, bathed by a medium whose initial temperature is the unperturbed local temperature θ_0 of the fireball. The air at the surface of the R.V. is assumed to radiate like a black body having the air surface temperature, θ_a. Asymptotically at late time the solution approaches a steady state having dependence on radial distance r from the R.V. as

$$\frac{\theta}{\theta_0} = 1 - \frac{ha}{\frac{r}{a}(ha + 1)}, \quad \text{where } h = \frac{3}{16\lambda_R},$$

and λ_R is the Rosscland mean free path. At the surface the temperature

depends on time t as

$$\frac{\Theta_a}{\Theta_o} = 1 - \frac{ha}{ha - 1} [1 - e^{x^2} erfc(x)] ,$$

where

$$x = (ha + 1)\sqrt{Kt/a^2} .$$

The parameter $K = \frac{\sigma\Theta_o^4}{hE}$ contains the black body emission flux $\sigma\Theta_o^4$ and the energy per unit volume E of the air at the unperturbed air temperature. A time τ, characteristic of the decrease in surface temperature from the initial value Θ_o, to the asymptotic value $\Theta_o/(ha+1)$, is given by

$$\tau = \frac{ha^2 E}{(ha+1)^2 \sigma\Theta_o^4}$$

Numerical evaluation of τ and $\frac{\Theta_o}{ha+1}$ shows that rather different conditions exist in the shock and radiative plateaus. In the former, the local cooling may be quite appreciable (for 90,000 ft, in the shock plateau at range 2.7×10^4 cm. Θ_s drops to $.3 \Theta_o$ and $\Theta_o = 1.5$ ev) but τ is rather long ($\tau = 3 \times 10^{-4}$ sec for the case above). Since the shock region contains large air velocities, which may be supplemented by the R.V. velocity, considerable convection occurs during this time, sufficient to increase markedly the asymptotic value (the displacement $d = v\tau$ is $d = 340$ cm with $v = 1.1 \times 10^6$ cm/sec. This is considerably greater than the assumed R.V. radius $a = 50$ cm and much greater than $\lambda_R = 4$ cm). In the radiative plateau the mean free path is longer principally because of decreased density so that the asymptote is much higher. On the other hand, the time τ is so short that convection is of no importance.(For 90,000 ft in the radiative plateau at range 2.5×10^4 cm, $\Theta_s = .88 \Theta_o$ and $\Theta_o = 5$ ev. $\tau = 1.2 \times 10^{-6}$ sec, giving $d = 1$ cm. Here $\sigma\Theta_s^4$ is reduced to 0.6 of the unperturbed medium value.)

For the cases investigated the effect of local cooling is neither larger nor completely negligible. Somewhat surprisingly, the effect is smaller at the 60,000 ft altitude where strong hydrodynamics decreases the density sharply behind the radiative front to a value actually lower than at a

comparable stage at 90,000 ft. At altitudes considerably higher than 90,000 ft, one would expect that the decrease of air density and increase of mean free path would reduce the effect to negligible proportions. At intermediate altitudes it appears to be necsssary to take into account some reduction of flux due to this effect.

C. HYDRODYNAMIC ENVIRONMENT

As the shock wave sweeps over the R.V. the Mach number of the air is initially large ($M_1 \sim 3$) and the stagnation point pressure against the R.V. is greater than ambient by a larger factor (~ 10). As the radiation front engulfs the R.V. the air velocity drops and the sound speed decreases to give a typically subsonic flow ($M_1 \sim .7$) and a small increase of stagnation pressure over ambient (~ 1.3). The pressure changes in the opposite sense on the surface away from the explosion center, of course. The velocity of the R. V. itself is not negligible compared with the air velocity and may add to or subtract from that of the air depending on the relative orientation of the R.V. in the explosion. While these dynamic effects are not small, the sign of the effect depends on R.V. orientation and surface of interest. The ambient pressure is, in a sense, the central value of the pressure.

III. NATURE OF THE INTERACTION

Calculations carried out with the code as described in Section I and with boundary conditions for the three cases recorded in Section II.A. are analyzed in this section. The properties assumed for the surface of the R.V. are those characteristic of a low thermal conductivity plastic composed of low-Z elements for which more data are recorded in Section I.G. For the purpose of taking into account the divergence of the expanding vapor as described in Section I.C. a characteristic R.V. radius $\bar{r}$ = 50 cm was used. In each case an outer layer of the plastic was divided into 150 zones, the outermost one of which was 10^{-3} gm/cm^2 in thickness. Zones increased in thickness with increasing depth into the surface to give a total zoned layer thickness of 0.5 gm/cm^2, or 0.5 cm at the initial density of 1.0 gm/cm^3.

Calculations were continued forward in time until from 1.5×10^{-3} to 4×10^{-3} sec had elapsed. This history corresponds to transit through the shock plateau and rise of source temperature toward its peak, stopping somewhat before achieving the peak source temperature. Impulse experienced by the R.V. in each of these cases by the time of problem termination was approximately 10^5 dyne-sec/cm^2.

Each problem required typically a little more than 2000 cycles or time steps and a little less than one hour of 7090 computer use. Calculations were rezoned to remove superfluous zones as often as twice per problem and in one of the problems (h = 90,000 ft, r = 2.5×10^4 cm) almost all of the mass provided in the mesh had been ablated by time of termination.

Results of the calculations are examined in the sections below. In Section A for one of the problems the spatial characteristics of temperature θ, pressure P, velocity v, density ρ, and Rosseland mean free path λ_R, are examined. A comparison between the radiation fluxes calculated with and without frequency dependence is also made. In Section B all three problems are analyzed for time dependence of impulse per unit area, I/A, and ablated mass per unit area, m_a. The coupling constant, $\dot{I}/\dot{Q}$, is also examined during the interaction history. Section C contains a comparison of two problems

differing only in the way source energy is deposited in vapor and solids. Finally, in Section D the conditions for convective instability are examined and estimates are made of the role it plays in the TME.

A. SPATIAL CHARACTERISTICS

In Figs. III-1 to III-20 profiles of five quantities are shown at four instants during the 90,000-ft explosion at interaction range = 2.5×10^4 cm. In Fig. III-1 the temperature at $t = 4.3 \times 10^{-4}$ sec is seen to be almost constant at 0.45 ev. At this time energy from the fireball streams through the cool vapor with very little absorption so that most of the source is deposited in the solid where it is very efficient in producing vapor. The boundary pressure at the interface is important in retarding the blowoff and in elevating the pressure on the solid above the free blowoff value. Also for this reason the blowoff velocity remains low and the vapor density relatively high. The limitation of the temperature at 0.45 ev is due to a combination of the large dissociation energy needed to reach higher temperatures and the small absorptivity of the vapor at low temperature. The energy absorbed from the source does, however, at $t \sim 6.3 \times 10^{-4}$ sec exceed the dissociation energy in the outside layers resulting in a marked temperature rise as shown in Fig. III-6. Accompanying the increase in temperature is an increase in vapor ionization and absorptivity which markedly affects the behavior of the problem. The solid suddenly is shielded from the source by the very opaque vapor which, in turn, is heated to a high enough temperature for reradiation to play a role. In Fig. III-11 at 8.0×10^{-4} sec the vapor temperature has reached 3.9 ev, sufficient to reradiate 35% of the incident energy from the system. The source is now being absorbed by the denser vapor at the head of the advancing temperature wave which is also radiating energy ahead into the cold vapor. Considerable hydrodynamic disturbance results from the rather sudden expansion of the previously cold vapor and impels a compression and shock wave forward. The hot vapor now expands outward with velocity $\sim 10^6$ but the cold vapor is recompressed against the solid.

In Fig. III-16 the temperature wave has progressed inward close to an equilibrium position in the vapor. Reradiation does not yet contribute appreciably to the ablation rate but will do so at a little later time. It is expected that on completion of the vapor heating a greater fraction of

source energy will reach the solid which, together with reradiation, will appreciably increase the ablation rate. Loss of energy from the system by reradiation still accounts for 38% of the source. At this time the inward-driven wave has reflected from the R.V. surface with pressure $p = 9 \times 10^7$ and is driving the vapor outward with $v > 2 \times 10^6$ cm/sec.

Throughout these problems the boundary pressure has ensured that the density remain high enough for the hot vapor to stay in the radiation diffusion regime. As a consequence of this, local thermodynamic equilibrium has been maintained throughout the entire calculation.

One calculation of the frequency-dependent radiation transport was also made on the above problem. Corresponding to $t = 8.5 \times 10^{-4}$ sec, the calculation permits comparison with the transport calculation using the Rosseland mean free path as employed for the entire histories of the time-dependent calculations. At this time, as noted above, the temperature profile consists of a high temperature plateau, an abrupt transition region, and a low-temperature plateau into which radiation streams from the hot region. In Fig. III-21 the radiative fluxes calculated in these two ways are shown throughout the system. At the outer boundary the flux is positive, corresponding to black body emission from the high temperature plateau. Deeper into the vapor the flux decreases and changes sign as the region of transition is approached. This change of sign of flux is noted on the graph by a vertical line marking the position. In the negative flux region the flux reaches a minimum as the temperature falls and then rises again toward zero by absorption toward the solid. Good agreement is found in the high temperature regime. In the transition region, however, the Rosseland curve is too high while at the solid it is appreciably too low. In view of the smallness of the radiative flux compared to the source flux, very little error was made, showing that the Rosseland treatment is, in this case, quite satisfactory. For times when radiation contributes importantly to the ablation rate, more important deviation may be expected, however. Work now in progress on using the frequency-dependent code throughout the calculation may then be very valuable. In Fig. III-22 the frequency dependence of the flux is displayed at several positions in the vapor.

B. EVOLUTION IN TIME, LETHALITY, AND MATERIAL LOSS

During the interaction the pressure at the solid surface results in a continued increase of impulse contributed to by both the ambient pressure and the ablation pressure as influenced by the hydrodynamics of the vapor. The amount of mass ablated determined by source and reradiation also increases with time. In Figs. III-21 through III-23 the history of both of these quantities is shown for the three interaction problems. At early times in the shock plateau the curves are all very similar with approximately linearly increasing ablation and impulse with time. This phase is terminated by the progressive increase in source rate as the radiative wave arrives. Happening at earliest time in Problem 1 and successively in Problems 2 and 3, the ablation rate responds immediately, followed much more slowly by the impulse curve. Problem 3 was terminated in this state. The first two of the problems, however, show the effects of the catastrophic surface temperature increase reflected by sudden decrease in the mass ablation rate and in the impulse curve by a sudden drop in the ablation pressure, introducing a plateau in the impulse curve.

In Problem 2 the calculation was ended almost immediately after ionization started. Only in Problem 1 is this phenomenon followed farther. The mass ablation curve is greatly decreased in slope for an extended interval equal to at least 10^{-3} sec for Problem 1. In the impulse curve, however, structure is introduced by the violent hydrodynamic motions triggered by the reduction in ablation. Pressure at the solid interface is reduced at the same time that a shock wave is driven inward by the expanding material in the heating wave. These then cooperate to raise the pressure of the solid momentarily to $P > 10^8$ as the shock reflects. Consequently, the impulse curve rises abruptly and, after some smaller fluctuations, assumes a new slope smaller than the original. While Problem 1 was terminated before the thermal wave reached the solid, this event should initiate a new increase in both mass ablation rate and ablation pressure.

It is also of interest to examine the efficiency of the thermal energy source in producing impulse. This has been done by forming $I/E = d(I/A)/\dot{Q}dt$ where $\dot{Q}$ is the thermal power per unit area from the source $\dot{Q} = \sigma\theta_o^4$ in watts/cm^2. In Figs. III-24 through III-26, I/E, the instantaneous coupling

coefficient, is shown vs time for the three problems. The values are surprisingly large at early times in consequence of the fireball ambient pressure. This pressure, more conventionally thought of as part of the blast wave and associated with the blast regime, is relatively more important in the shock plateau before the ablation rate has risen. At the 60,000-ft altitude the interaction is almost entirely attributable to the blast regime with only minor TME superimposed. This altitude is clearly below separation boundary between blast and TME. At the altitude of 90,000 ft, however, blast and thermal effects are interwoven into a closely interrelated cumulative effect. The more specifically ablative values of I/E are obtained as the ablation pressure rises well above ambient. While considerable structure is introduced into the Problem 1 curve by vapor heating, typical values of I/E associated with the thermal mechanical effect appear to be 1-5.

Lethality. It is striking that, as a consequence of vapor shielding Problem 1 at a shorter range from the explosion has less ablation than and comparable impulse to Problem 2 after 1.5×10^{-3} sec of interaction. The impulse curve for Problem 2 is considerably steeper and thus more damaging, although both locations have probably suffered lethal damage. (Lethality is evaluated in terms of criteria established by Abrahamson and Lindberg.[11] These require total impulse per unit area $> 2 \times 10^4$ and pressure $> 4 \times 10^7$.) The vapor shock in Problem 1, however, is worthy of further investigation as to its lethality. The impulse curve for h = 60,000 ft in Problem 3 is considerably shallower corresponding to lower pressure which is probably not lethal to a hardened R.V.

Material Loss. The amount of material lost by ablation is not large during the calculations. If the rate of ablation were maintained near its peak value for the duration of the high temperature, however, significant material loss would result.

C. COMPARISON OF SOURCE FUNCTIONS

While for an isotropic incident distribution the correct law of decrease of flux at optical depth x below the surface is given by $2E_3(x)$ (see Section I.A. for a description of the source subroutine), an early version of the source erroneously contained $E_2(x)$. While these functions lead to the same

total incident flux, the latter function deposits the energy nearer the surface than the former. Since some of problem h = 90,000, r = 2.5 x 10^4 was run with E_2 before being repeated with $2E_3$, a comparison exists between problems differing only in the angular distribution of the source or equivalently in the deposition function for the source energy. This comparison gives an indication of the sensitivity to depth of deposition of results and, consequently, gives some basis for judgement of how accurately the non-isotropic distribution at higher altitudes must be approximated. In Fig. III-27 the impulse per unit area and mass ablated are compared at rather early times. While initially the curves are substantially the same with all of the energy penetrating to the solid, as vapor is evolved the E_2 function deposits more energy in vapor, leaving less for vaporization. The greater deposition in the vapor at the air interface supplies the dissociation energy there at an appreciably earlier time and initiates the catastrophic heating and ionic absorption which, in turn, is the reason for the reduction in rate of increase of impulse and mass ablation. Since these phenomena occur at earlier time, source rate, and total energy the E_2 deposition reduces the interaction considerably. It is not known, of course, whether the earlier completion of the vapor heating would result in a compensating earlier resumption of strong ablation. The differences in Fig. III-27, however, occur at a significant part of the interaction in that the impulse is increasing most rapidly there and are of sufficient magnitude to indicate considerable sensitivity of results to angular distribution. Some care in specifying the distribution is indicated. The same may be said of the low temperature vapor absorption coefficient, pointing up the need for more accurately known material properties.

D. CONVECTIVE INSTABILITY

There is theoretical evidence that radiation is not the only energy transport mechanism present in the vapor when the temperature reaches values large enough to make radiation itself an important process. The additional transport mechanism is one which takes place if elements (bubbles) in the gas may be convected by the acceleration field to increasingly greater distances from their point of origin. Only if the motion is unstable does the convection establish a non-zero steady state in which energy is convected.

An analog of this process is convective heat transfer in the atmosphere where the buoyancy displacement of air cells may under certain conditions be unstable. There is experimental evidence from the Orion investigations indirectly applicable to the thermal interaction, that the process is present in a similar radiative ablation environment.

Consider a slab of material with a positive pressure gradient and with a density and temperature gradient as shown below.
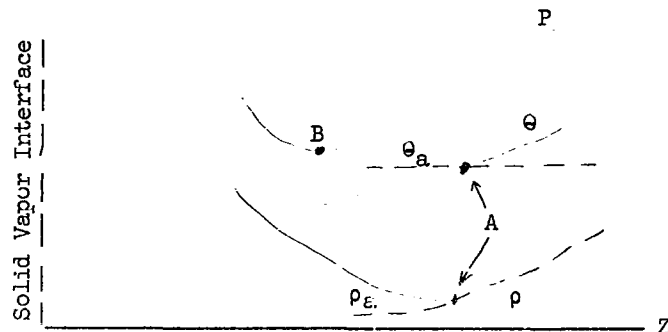
The two curves labeled Θ_a and ρ_a indicate the way in which the temperature and density would vary if from point A the flow were adiabatic and the pressure remained the same. If a perfect gas equation of state is assumed, $P = \alpha\rho\Theta$, then along $P = K\rho^\gamma$, the adiabat is determined by P:

$$\rho_a = \left(\frac{P}{K}\right)^{1/\gamma}, \quad \therefore \left.\frac{\partial\rho}{\partial z}\right|_a = \frac{\rho}{\gamma P}\frac{\partial P}{\partial z}$$

and

$$\Theta_a = \frac{K}{\alpha}\left(\frac{P}{K}\right)^{1-\frac{1}{\gamma}}, \quad \therefore \left.\frac{\partial\Theta}{\partial z}\right|_a = \left(\frac{\gamma-1}{\gamma}\right)\frac{\Theta}{P}\frac{\partial P}{\partial z}.$$

A small element of vapor displaced to the left from A along the adiabat experiences an unbalanced force on the element proportional to

$$\left[-\frac{\partial P}{\partial z}\left(\left.\frac{\partial\rho}{\partial z}\right|_a - \frac{\partial\rho}{\partial z}\right)\right]$$

If the quantity given in the brackets is negative, then the element will continue to move to the left and the vapor will be unstable to small perturbations. An element displaced to the right from B will be unstable with

respect to displacement to the right under the same conditions. The result is convective energy transfer toward the solid vapor interface due to the circulation in the unstable layer of hot elements toward the colder region and cold elements toward the hotter region. The condition for instability can be written as

$$\frac{\partial P}{\partial z} \left(\frac{\partial \theta}{\partial z} \bigg|_a - \frac{\partial \theta}{\partial z} \right) < 0 .$$

Convective energy transport in an unstable layer in the presence of energy transport by radiation is also well known in stellar interiors.[12] A similar energy flow has been observed in fluids in the presence of thermal heat conduction[13] where the convective mixing cells that are formed are known as Bénard cells.

The energy flux in the unstable layer can be estimated in two ways. Schwarzschild[12] derives a convection flux that is given by

$$\phi_c = \rho C_p = \Delta \left(\frac{\partial \theta}{\partial z} \right) \left[- \frac{\partial P}{\rho \partial z} \cdot \frac{1}{\theta} \Delta \left(\frac{\partial \theta}{\partial z} \right) \right]^{\frac{1}{2}} \frac{\ell^2}{4}$$

where

$$\Delta \left(\frac{\partial \theta}{\partial z} \right) = \frac{\partial \theta}{\partial z} \bigg|_a - \frac{\partial \theta}{\partial z}$$

and ℓ is the mixing length. This quantity can be estimated to be the width of the unstable layer.

In Ref. 13 the effect of viscosity in the Bénard cell problem is considered. It is shown that the energy flux is unchanged until a critical value for a dimensionless number, the Rayleigh number (R), is reached in the layer. A Rayleigh number can be defined for the radiation environment as

$$R = \frac{C_p}{\phi_{Rad}} \frac{\partial \theta}{\partial z} \cdot \frac{\partial P}{\partial z} \cdot \frac{\partial \rho}{\partial z} \cdot \frac{1}{\eta} (\ell)^4$$

where ϕ_{Rad} is the radiative flux and η is the viscosity. The ratio of energy transfer with the instability present to the energy transfer in the absence of convective mixing, the Nusselt number (Nu), has been measured as a function of R for the Bénard experiment. The results are independent of the fluid used in the experiment. The critical value of R for the experiment reported is ~ 1600. The Nusselt number is observed to be a very weak function of R, e.g., for $R = 10^9$, $Nu = 8$.

Fig. III-1

34

Fig. III-2

Fig. III-3

Fig. III-4

Fig. III-5

Fig. TTT-6

Fig. III-7

Fig. III-8

Fig. III-9

Fig. III-10

Fig. III-11

44

Fig. III-12

Fig. III-13

Fig. III-14

Fig. III-15

Fig. III-16

49

Fig. III-17

Fig. III-18

Fig. III-19

Fig. III-20

Fig. III-21--Comparison of Fluxes
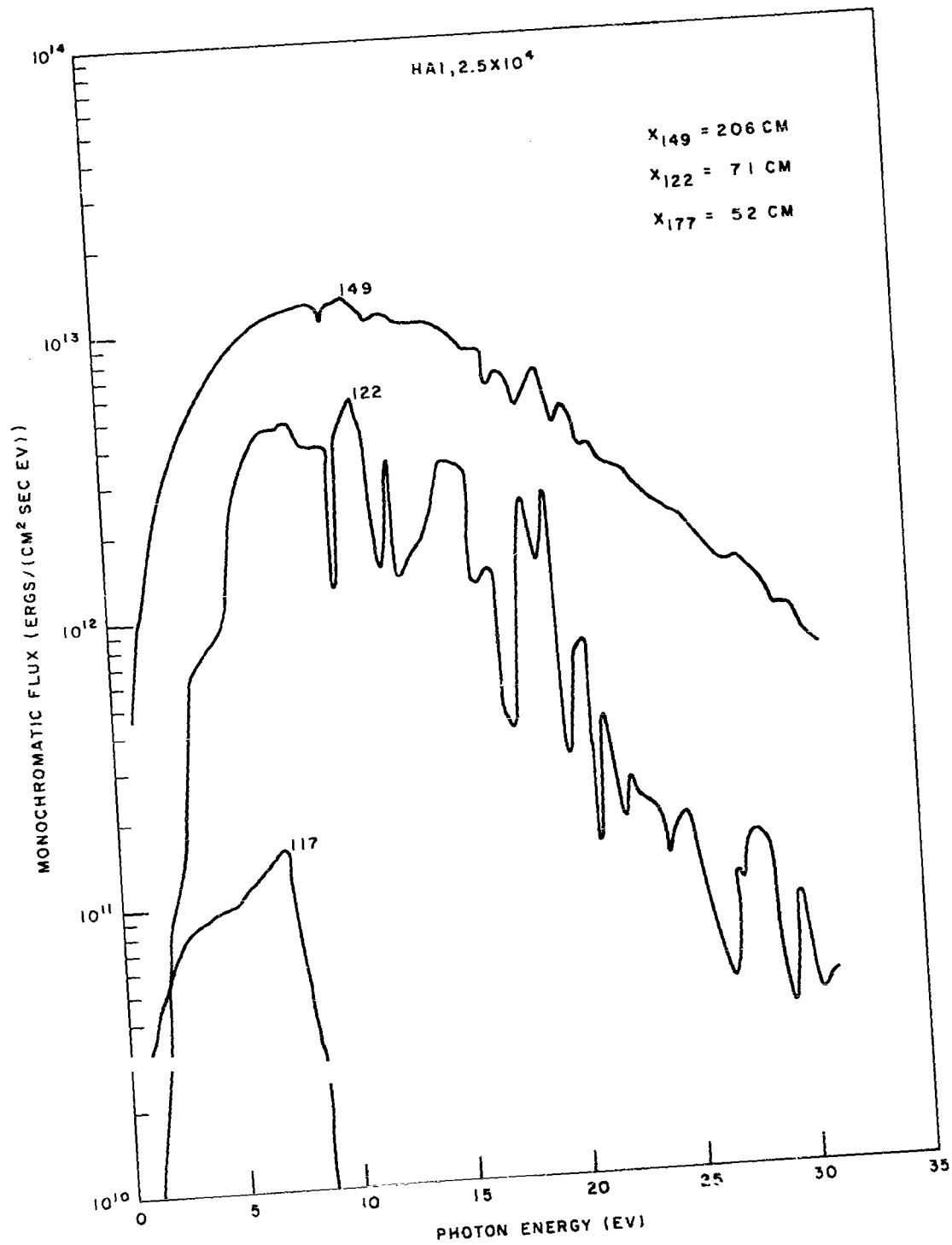
Fig. III-22--Fluxes vs Frequency
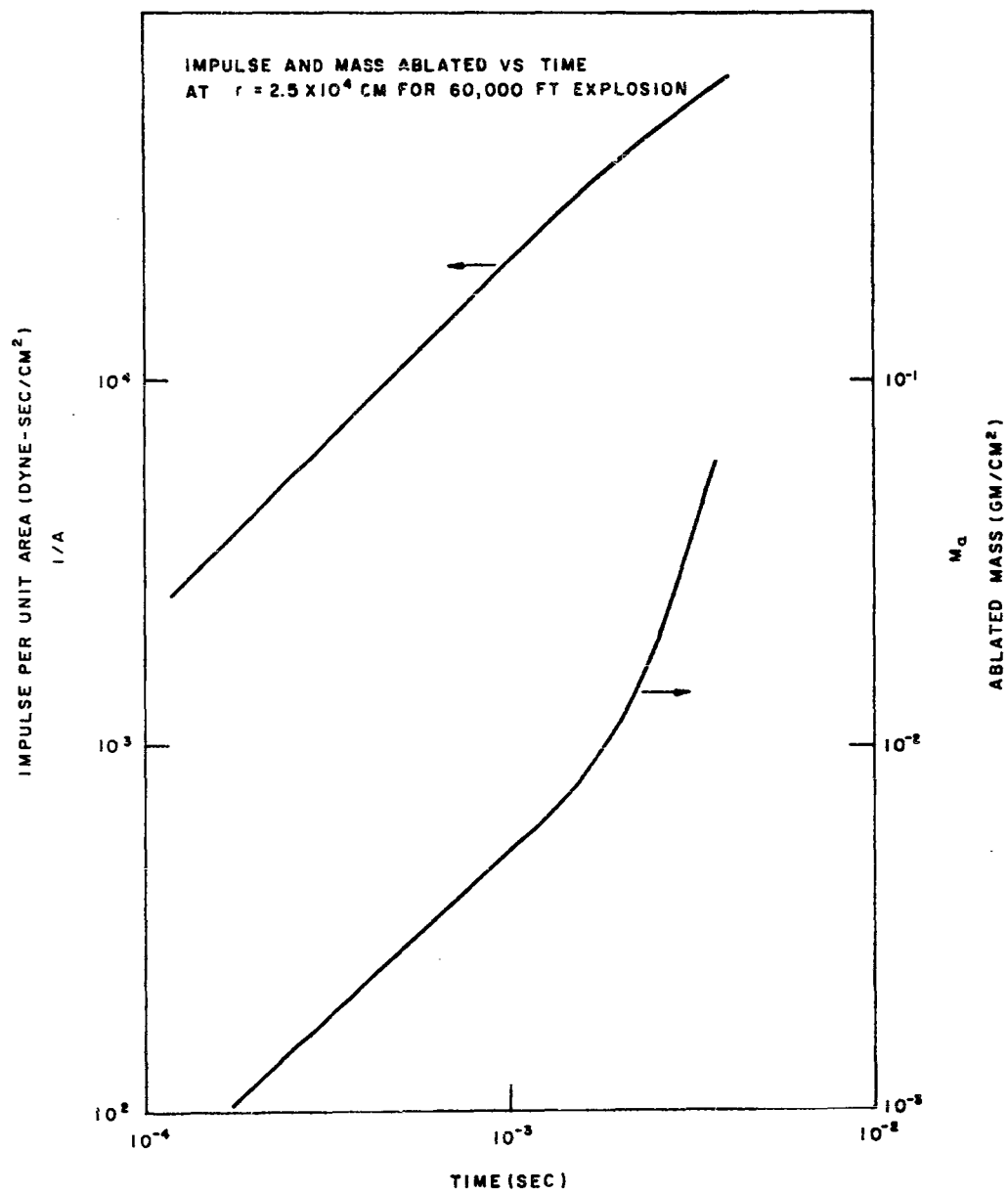
Fig. III-23

IMPULSE AND MASS ABLATED VS TIME
AT   r = 3.0 X 10⁴ CM FOR 90,000 FT EXPLOSION

Fig. III-24

Fig. III-25

Fig. III-26 — $\dot{I}/Q$

COMPARISON OF E_2 AND E_3
SOURCE DEPOSITION FUNCTIONS
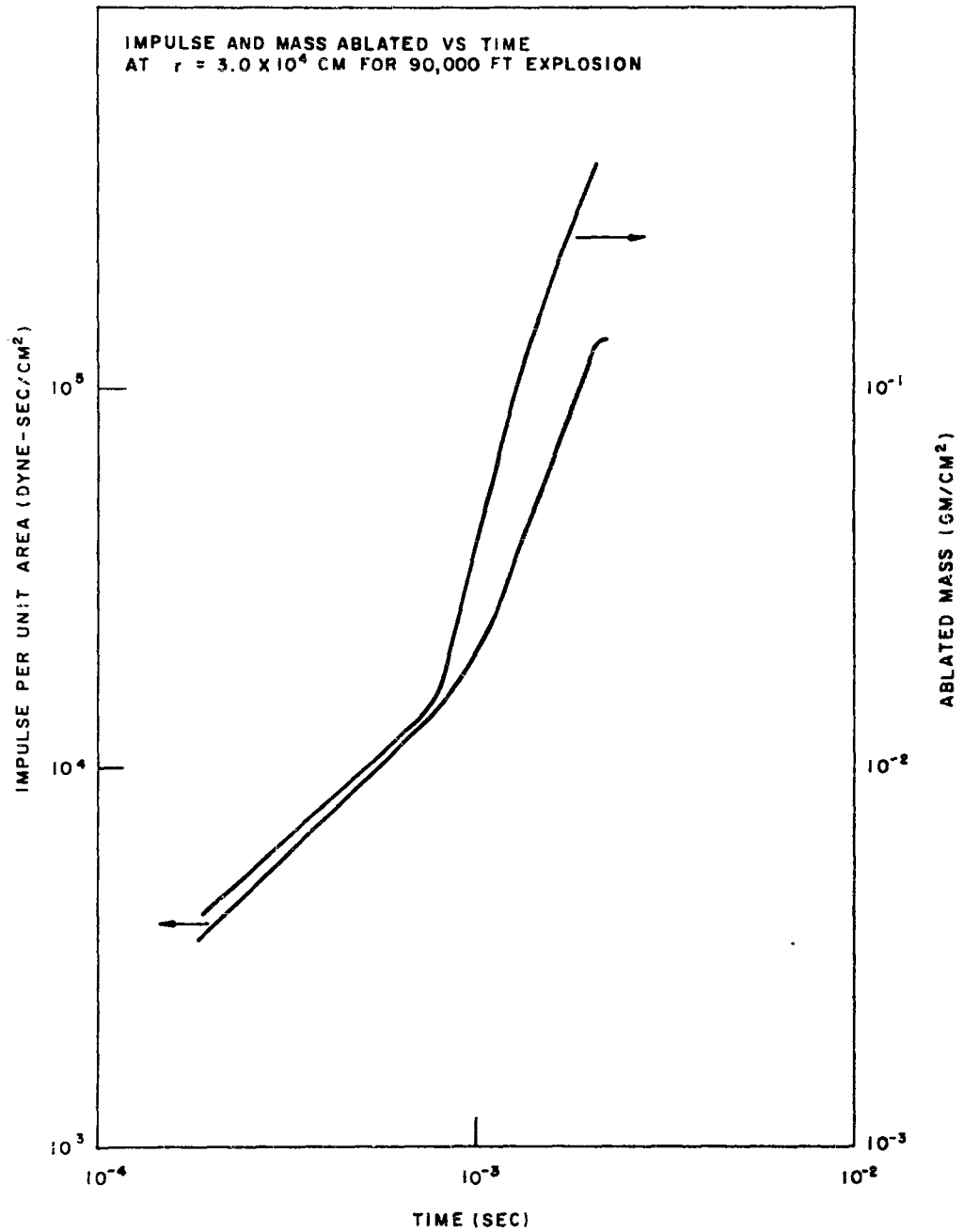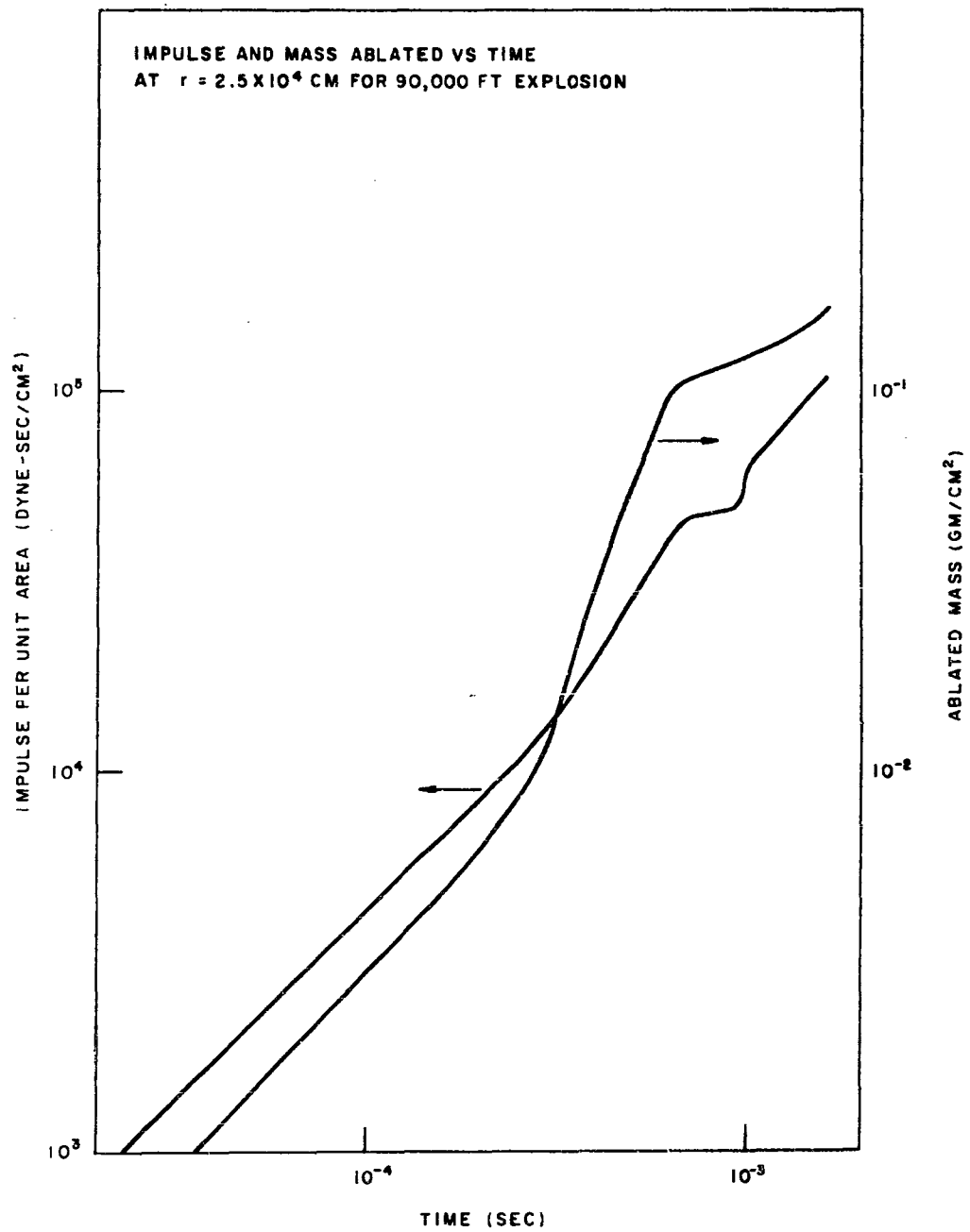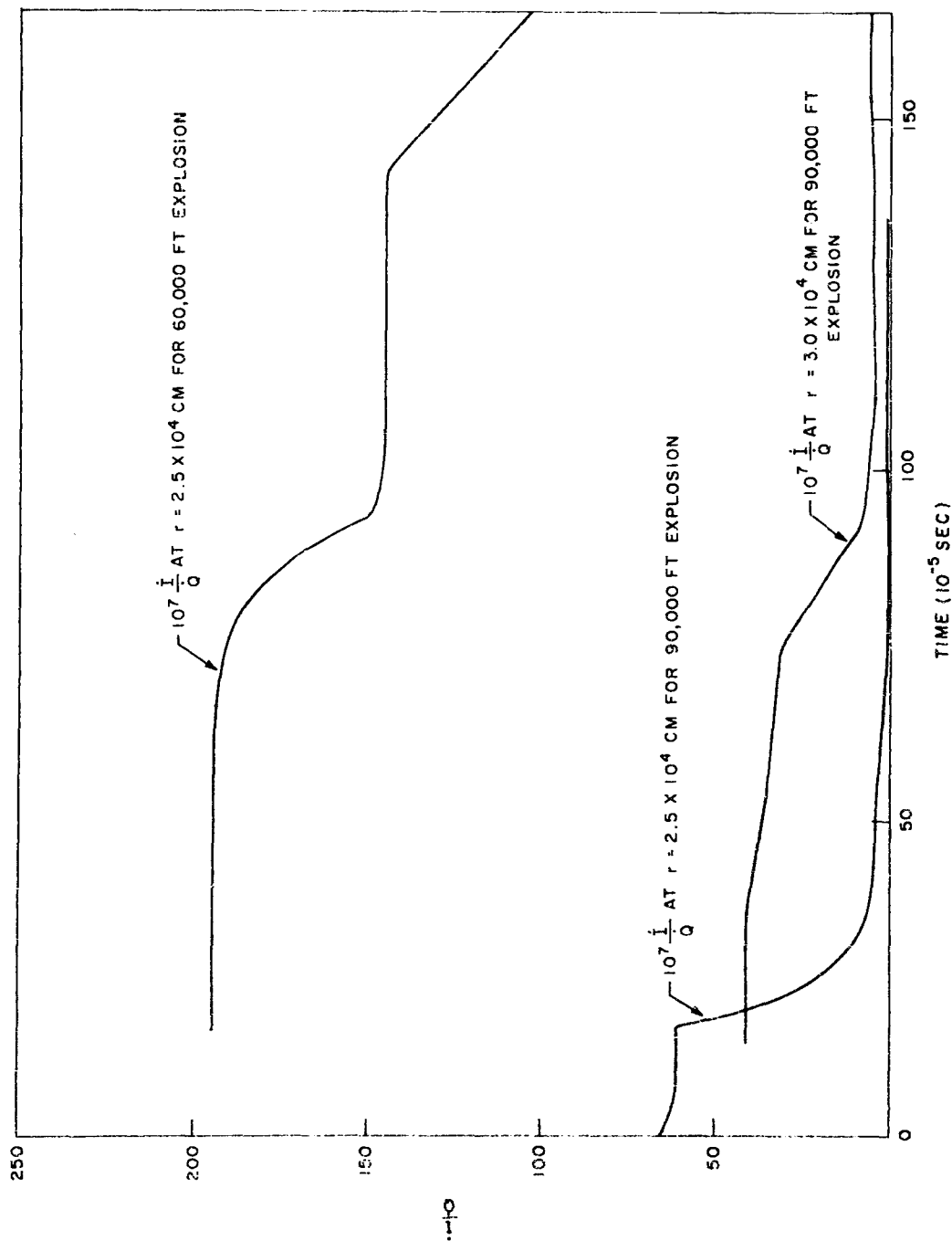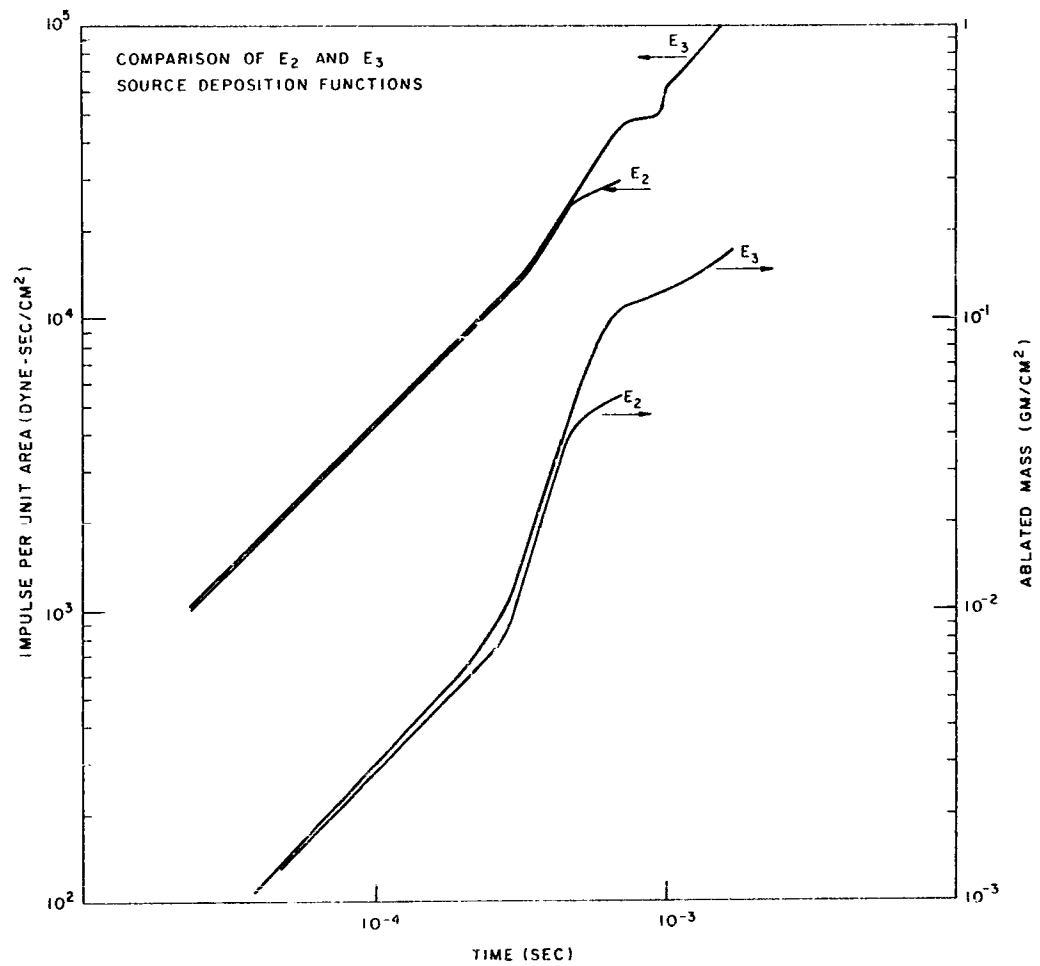
Fig. III-27--Comparison of Source Angular Distributions

REFERENCES

1. General Atomic proposal GACP-4290, Proposal for a Program on Fireball Phenomenology Code Development (U), Appendix B, May 1963 (S/RD).

2. Freeman, B. E., "Source Routine for Calculations of the Thermal Mechanical Effect" (U), GAMD-4275, May 1963 (S/DI).

3. Pyatt, K. D., Jr., "First Semiannual Technical Summary Report on Contract AF29(601)-5695, GA-3829, January 1963 (S/DI).

4. General Atomic proposal GACP-3221, Proposal for Theoretical Study on Interaction of Laser Radiation with Matter" (S/DI), June 1962 (S/DI).

5. Stewart, J. C. and K. D. Pyatt, Jr., "Theoretical Study of Optical Properties", Vols. I, II, III, GA-2528 (SWC-TR-61-71), September 1961 (Uncl).

6. Freeman, B. E., "Numerical Method for the Radiation Transport Equation in Plane Geometry", GAMD-2874, January 1962 (Uncl).

7. Bernstein, J. and F. J. Dyson, "Continuous Opacity of Light Elements at Low Densities", GA-848, July 1963 (Uncl).

8. Unpublished calculations of mixtures of elements have used the same technique and code as for the low-Z elements reported in Ref. 5.

9. Davis, C. G., "Numerical Calculation of a Nuclear Explosion at High Altitude" (U), GAMD-4301, June 1963 (S/RD).

10. Davis, C. G. and B. E. Freeman, "Calculation of Early Time Nuclear Formation and Growth" (U), GA-4349, Final report on Contract AF29(601)-6025, June 1963 (S/RD).

11. Abrahamson, G. R. and H. E. Lindberg, "Ultimate Structural Hardness of Reentry Vehicles" (U), Preliminary report on Contract AF29(601)-4745, June 1963 (S/DI).

12. Schwarzschild, M., Structure and Evolution of the Stars, Princeton, N.J., Princeton University Press, 1958.

13. Chandrasekhar, S., Hydrodynamic and Hydromagnetic Stability, London, Oxford University Press, 1961.

APPENDIX A

THERMAL SOURCE FLOW DIAGRAM AND CODE

The quantities required as input for the "QUE" and "HYDRO" subroutine are given below, together with descriptions.

HYDRO

D(J)   Fractional weights of a finite number of frequency groups for the source.

CRTPC(J)   Average energies of a finite number of frequency groups for the source.

CHRNO(24)   Number of frequency groups of the source.

CHRNO(25)   Constant coefficient used for the CAPAC(I) calculation.

RDK(1-52)   Times (t_i) for the QUE subroutine.

RDK(53-104)   Initial boundary temperatures (Θ_L) for the QUE subroutine.

SOLID(1)   Positive, zero or negative trigger to use EXPI4, EXPI3, or EXPF in source angular distribution.

SOLID(2)   Cosine of angle of incidence of source ray, μ_o, usually one.

SOLID(3)   Constant factor, ≤ 1, to represent a distant thermal source.

SOLID(8)   Initial source rate used to establish conduction wave.

SOLID(9)   Constant coefficient used for the XKLC calculation.

A   Atomic number of target material.

Z   Charge number of target material.

QUE

THETAK(1-52)   Times (t_i) for the pressures in "hydro".

THETAK(53-104)   Boundary pressures $(\Theta_i$ in "hydro".

IB = SUMRB — Set up left-hand boundary of vapor.

DO
I = IB,
IBM1

Set 0 to fluxes.

GOFR(1) = 0

SUMRB = IB — Initialize identification storage for zone of deepest source penetration.

(1500)

(180)

RDK(1) ≥ RDK(1)-TH ····· (161)

<
(180)

Interpolate linearly among t_J, θ_J to obtain the source temp. θ_o.
Source = 0 if TH > t_J.

DO
J=2, 52

J = J

RDK(J) - RDK(J-1) ≤ RDK(J) = S6=0.
160   SOLID(8)=0.
161

RETURN
1000

TEMP(1)=RDK(J+52) ← RDK(J)-TH > TEMP(1)=RDK(J+51)+(RDK(J+52)-RDK(J+51))/ (RDK(J)-RDK(J-1)*(TH-RDK(J-1))

<
CONTINUE →(160)

GO TO 200

WRITE OUTPUT TAPE 6, 190, RDK(J), J

FORMAT (1941 INPUT THETA ERROR, 1PE 15.7, I4

CALL UNCLE →(200)

<
>

(33)

$$SV(IAM1) = SOLID\ (27)$$

$$NBOIL = 2$$

$$A(I) = \frac{A(I)[1. - SOLID\ (24)]}{SOLID\ (24)}$$

Boiling zone is being calculated. Set up quantities to evaluate optical depth of vaporized fraction of boiling zone. Exit to form optical depth contribution at **(3)**.

(3) **(37)**

$$A(I) = A(I) \cdot SOLID(24)$$
$$SV(IAM1) = TEMP(4)$$

Restore boiling zone quantities.

(5)

$$q(I) = [GOFR(I+1) - GOFR(I)] \cdot \dot{E}$$

Zone source is formed

$$\left(GOFR(I) - 10^{-4}\right) < \qquad q(I) = q(I) + GOFR(I) \cdot \dot{E}$$

Add remaining energy to last zone

$\geq$

$$(1 - I) \leq \qquad \dot{E} \cdot \dot{E}(1.-GOFR(I))$$

Throw away energy which penetrates the entire mesh.

$$I = I - 1$$

Do next zone inward from surface.

(4)

$$SUMRB = I$$

Record last zone

$$RPIB = RPIB + \dot{E}\Delta t_H$$

Tally energy added on cycle and return to main code.

RETURN

(3)

XKLC = SOLID(9)/SV(1)   Form low temperature absorption coefficient.

FEW(I) $\leq$ $$TEMP(11) = \frac{XKLC \cdot g(I)}{A(I)}$$ If vapor is unionized, form optical depth and normalized flux from low temperature absorption coefficient.

$>$

Find what material is in zone I.

DO
K = I
MAXIM

DO
I=1, iK

$(I - IMDA(K+1)) \quad >$ CONTINUE

PB(J) = PB(J) + TEMP(11)

IF = K $\leq$

$$u_1 = \frac{13.6[Z(IF)]^2}{\theta(1)}$$

TEMP(2) = EXPI3(PB(J))
TEMP(2) = TEMP(2)+TEMP(2)
GO TO 512

TEMP(2) = 3.*EXPI4(PB(J))   SOLID(1)   0

$$\Gamma = \frac{10^{-2}\theta(1)^{1.5} \cdot SV(1) \cdot A(IF)}{\langle Z \rangle}$$ Frequency-independent part of Raizer absorption coefficient.

TEMP(2) = SOLID(2)*
EXPF(-PB(J)/SOLID(2))

GO TO 512

$u_K = MINIF(u_1, \rho n_e \Gamma)$

$$CAPAC(I) = \frac{CHRNO(25) \cdot max(1., \langle Z \rangle)}{A(IF) \cdot \theta(1)^2 \cdot \Gamma}$$

COFR(1)=TEMP(2)*D(J)+COFR(I)
512

(513)

$$u = \frac{CRTPC(J)\Theta_O}{\Theta(I)}$$

$$u - uk$$

$$\text{TEMP}(2) = \frac{CAPAC(I)}{u^3}(e^u - 1) + 0.2$$

Form frequency-dependent part of absorption coefficient and sum all group contributions to optical depth and flux. Linear interpolation between low temperature and ionic coefficients when ⟨Z⟩ < .5

$$\text{TEMP}(2) = \frac{CAPAC(I)}{u^3}(1 - e^{-u})e^{uk} + 0.2$$

$$.5 - Z$$

$$\text{TEMP}(2) = (⟨Z⟩ \cdot \text{TEMP}(2) + (.5 - ⟨Z⟩) \cdot XKIC) \cdot 2.0$$

$$PB(J) = \frac{\text{TEMP}(2) \cdot g(I)}{A(I)} + PB(J)$$

SOLID(1)

TEMP(2)=SOLID(2)*
EXPF(-PB(J)/SOLID(2))
GO TO 410

TEMP(2)=EXPI3(PB(I))
TEMP(2)=TEMP(2)+TEMP(2)
GO TO 410

TEMP(2)=3.*EXPI4(PB(J))

$$GOFR(I) = \text{TEMP}(2)*D(J) + GOFR(I)$$
410

Determine whether a boiling zone is being calculated and return to proper location.

```
          IL=SUMRB
          DO 1 I=IL,IBM1
     1 GOFR(I)=0.
          SUMRB=IB
C         T(I) GREATER THAN OR EQUAL TO ZERO
C         T(I+1) GREATER THAN OR EQUAL TO T(I)
          IF (RDK(1)) 180,110,110
   110 IF (RDK(1)-TH) 120,120,161
   120 DO 135 J=2,52
          J=J
          IF (RDK(J)-RDK(J-1)) 170,170,130
   130 IF (RDK(J)-TH) 135,150,140
   135 CONTINUE
          GO TO 160
   140 TEMP(1)=RDK(J+51)+(RDK(J+52)-RDK(J+51))/(RDK(J)-RDK(J-1))*
      1(TH-RDK(J-1))
          GO TO 200
   150 TEMP(1)=RDK(J+52)
          GO TO 200
   160 S6=0.
   161 SOLID(8)=0.
          GO TO 1000
   170 IF (RDK(J)) 180,160,180
   180 WRITE OUTPUT TAPE 6,190,RDK(J),J
   190 FORMAT(19H1 INPUT THETA ERROR,1PE15.7,I4)
          CALL UNCLE
   200 SOLID(8)=1.026E12*SOLID(3)*TEMP(1)**4
          GOFR(IB)=1.
          IK=CHRNO(24)
          DO 30 J=1,IK
    30 PB(J)=0.
          I=IBM1
     4 IF(BOILA)31,3,31
    31 IF(I-IAM1)3,32,3
    32 TEMP(4)=SV(IAM1)
          SV(IAM1)=SV(IAM1-1)
          NBOIL=1
          A(I)=A(I)/(1.-SOLID(24))
          GO TO 3
    33 SV(IAM1)=SOLID(27)
          NBOIL=2
          A(I)=A(I)/SOLID(24)*(1.-SOLID(24))
          GOFR(I)=0.
          GO TO 3
    37 A(I)=A(I)*SOLID(24)
          SV(IAM1)=TEMP(4)
     5 SMLQ(I)=(GOFR(I+1)-GOFR(I))*SOLID(8)
          IF(GOFR(I)-.0001)10,27,27
    27 IF(I-1)29,29,9
    29 SOLID(8)=SOLID(8)*(1.-GOFR(I))
```

```
          GO TO 28
     9 I=I-1
          GO TO 4
    10 SMLQ(I)=SMLQ(1)+GOFR(I)*SOLID(8)
    28 SUMRB=I
          RPIB=RPIB+SOLID(8)*DTH2
  1000 RETURN
     3 XKLC=SOLID(9)/SV(I)
          IF(FEW(I)) 511,511,509
   511 TEMP(11)=XKLC/A(I)*G(I)
          DO 512 J=1,IK
          PB(J)=PB(J)+TEMP(11)
          IF(SOLID(1)) 420,421,422
   420 TEMP(2)=SOLID(2)*EXPF(-PB(J)/SOLID(2))
          GO TO 512
   421 TEMP(2)=EXPI3(PB(J))
          TEMP(2)=TEMP(2)+TEMP(2)
          GO TO 512
   422 TEMP(2)=3.*EXPI4(PB(J))
   512 GOFR(I)=TEMP(2)*D(J)+GOFR(I)
          GO TO 513
   509 DO 610 K=1,MAXLM
          IF(I-LMDA(K+1))510,510,610
   510 IF=K
          GO TO 630
   610 CONTINUE
   630 TEMP(13)=13.6*CHRNO(IF)**2/THETA(I)
          TEMP(14)=THETA(I)**1.5*SV(I)/FEW(I)*1.E10/AMASNO(IF)
          TEMP(15)=LOGF(TEMP(14))
          TEMP(12)=MIN1F(TEMP(13),TEMP(15))
          CAPAC(I)=CHRNO(25)*FEW(I)*MAX1F(1.,FEW(I))
         1*AMASNO(IF)/(THETA(I)**2*TEMP(14))
          DO 40 J=1,IK
          TEMP(11)=CRTPC(J)*TEMP(1)/THETA(I)
          IF(TEMP(11)-TEMP(12))800,950,950
   800 TEMP(2)=CAPAC(I)/TEMP(11)**3*(EXPF(TEMP(11))-1.)+.2
          GO TO 35
   950 TEMP(2)=CAPAC(I)/TEMP(11)**3*(1.-EXPF(-TEMP(11)))*
         1EXPF(TEMP(12))+.2
    35 TEMP(11)=.5-FEW(I)
          IF(TEMP(11))39,39,38
    38 TEMP(2)=(FEW(I)*TEMP(2)+TEMP(11)*XKLC)*2.
    39 PB(J)=TEMP(2)/A(I)*G(I)+PB(J)
          IF(SOLID(1)) 400,401,402
   400 TEMP(2)=SOLID(2)*EXPF(-PB(J)/SOLID(2))
          GO TO 410
   401 TEMP(2)=EXPI3(PB(J))
          TEMP(2)=TEMP(2)+TEMP(2)
          GO TO 410
   402 TEMP(2)=3.*EXPI4(PB(J))
```

```
410 GOFR(I)=TEMP(2)*D(J)+GOFR(I)
 40 CONTINUE
513 IF(BOILA) 36,5,36
 36 IF(I-IAM1)5,11,5
 11 GO TO (33,37),NBOIL
    END
```

NO. OF CARDS

APPENDIX B

PRESSURE BOUNDARY CONDITION FLOW DIAGRAM AND CODE

SUBROUTINE HYDRO


```
        (10)

(PUSHA) = | IC = IA | ······> (PUSHB) =

P(IB) = TEMP(1)                P(IAM1) = TEMP(1)
IC = IAP1                      RD(IB) = ASMLR
C(IA) = R(IA)                  RIB = R(IB)
C(IAM1) = R(IAM1)              CB = C(IB)
                               G(IB) = 2.*(GL-SOLID(30))

     (IBP1-IC)

      DO                ERROR <  (THETAK(2))  >  P(IB) = TEMP(1)
    I=IBP1,
      IC
                                              CONTINUE
                                                 50
   R(I)=R(I)+RD(I)*DTH2
                                                 DO
                                               I=IC,IB
     (IB - IA)  >
                                               C(I)=R(I)
      ≤
    RETURN                          RD(I)=RD(I)+(2.*(P(I-1))/
                                    G(I)+C(I-1)*A(I))*DTH1

                                    R(I)=R(I)+RD(I)*DTH2

                                              CONTINUE
                                                 110
```
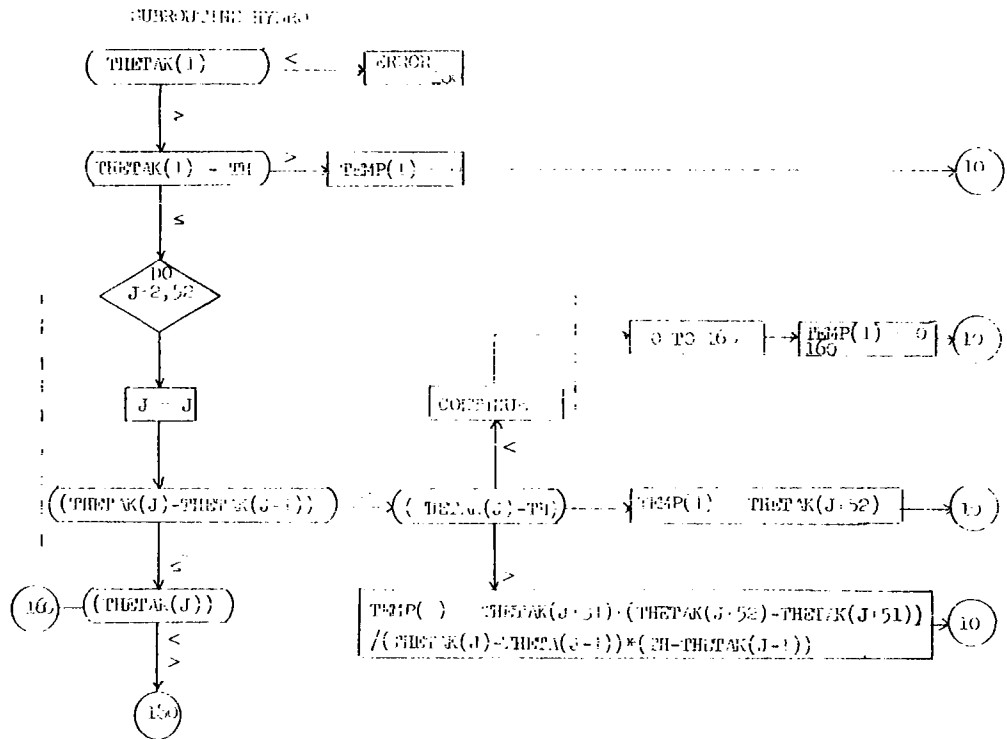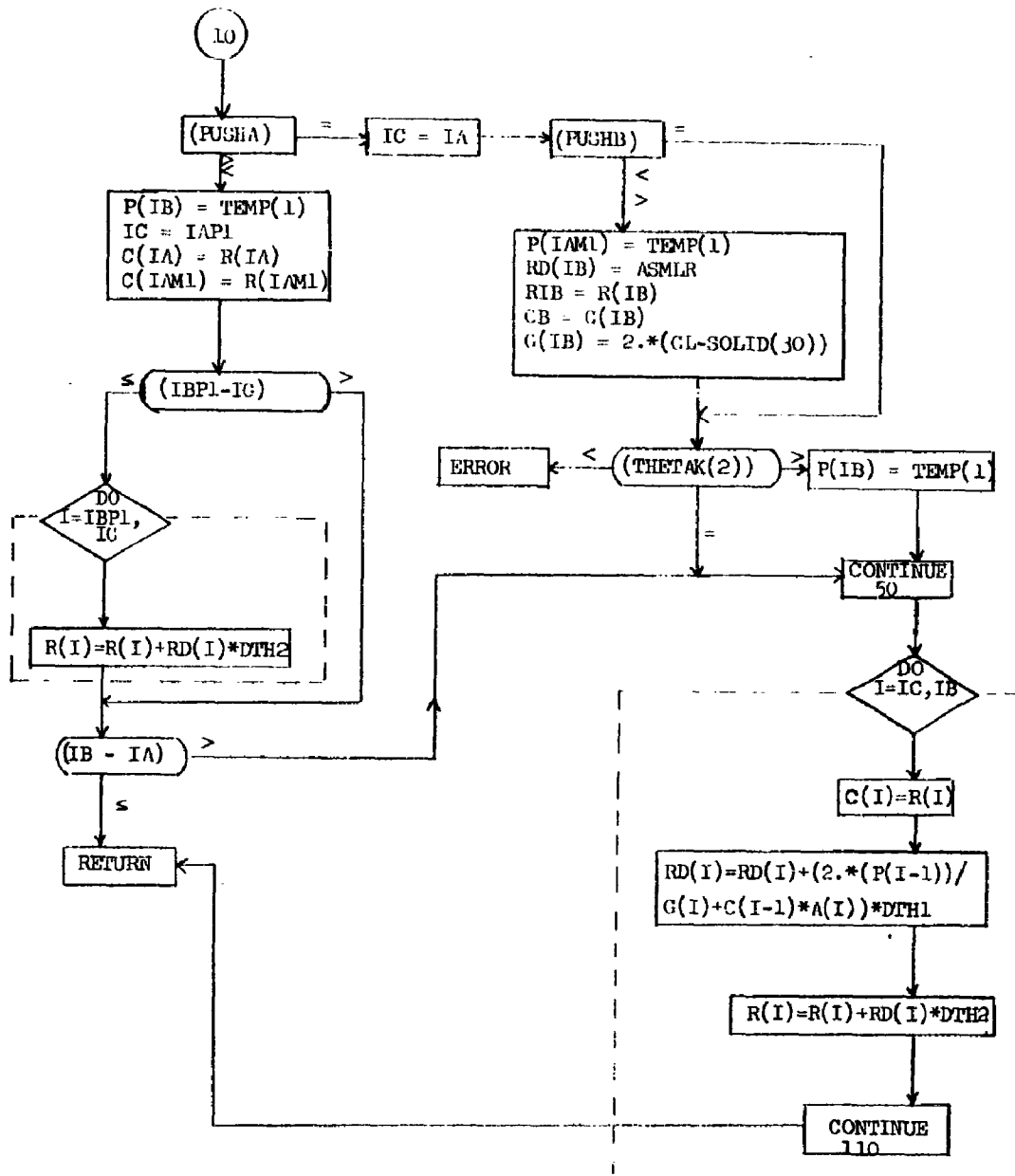
```
      IF (THETAK(1)) 180,100,100
100   IF (THETAK(1)-TH) 115,115,160
115   DO 135 J=2,52
      J=J
      IF (THETAK(J)-THETAK(J-1)) 170,170,130
130   IF (THETAK(J)-TH) 135,150,140
135   CONTINUE
      GO TO 160
140   TEMP(1)=THETAK(J+51)+(THETAK(J+52)-THETAK(J+51))/
     1(THETAK(J)-THETAK(J-1))*(TH-THETAK(J-1))
      GO TO 10
150   TEMP(1)=THETAK(J+52)
      GO TO 10
160   TEMP(1)=0.
      GO TO 10
170   IF (THETAK(J)) 180,160,180
180   WRITE OUTPUT TAPE 6,190,THETAK(J),J
190   FORMAT(22H1 INPUT PRESSURE ERROR,1PE15.7,I4)
      CALL UNCLE
10    IF (PUSHA) 11,20,11
11    P(IB)=TEMP(1)
      IC=IAP1
      C(IA)=R(IA)
      C(IAM1)=R(IAM1)
      IF (IBP1-IG) 12,12,14
12    DO 13 I=IBP1,IG
13    R(I)=R(I)+RD(I)*DTH2
14    IF (IB-IA) 120,120,50
20    IC=IA
      IF (PUSHB) 40,30,40
40    P(IAM1)=TEMP(1)
      RD(IB)=ASMLR
      RIB=R(IB)
      GB=G(IB)
      G(IB)=2.*(GL-SOLID(30))
30    IF (THETAK(2)) 180,50,31
31    P(IB)=TEMP(1)
50    CONTINUE
80    DO 110 I=IC,IB
      C(I)=R(I)
      RD(I)=RD(I)+(2.*(P(I-1)-P(I))/(G(I)+G(I-1))*A(I))*DTH1
      R(I)=R(I)+RD(I)*DTH2
110   CONTINUE
120   RETURN
      END
```

NO. OF CARDS

APPENDIX C

PROPERTIES OF CH_2

The DIAPHANOUS data are arranged in ascending values of the temperature as the first independent variable for each of which the second independent variable is the density arranged in descending sequence. Each page contains values for a single temperature (ev) and lists for reference the integrated black body thermal power $\sigma\theta^4$ (ergs/cm^2sec). In the body of the table the following quantities are tabulated:

Quantity	Units	Explanation	Formula
RHO	gm/cm^3	Material density	ρ
log RHO	-	Natural logarithm of density	-
Pressure	ergs/cm^3	Material pressure	P
ENERGY	ergs/gm	Total specific material energy	E
EION	ergs/gm	Ionic specific material energy	-
ZBAR	-	Number of free electrons per atom	-
EGAM	-	Strong shock "gamma"	$\gamma = 1 + \dfrac{P}{\rho E}$
KROS	cm^2/gm	Rosseland mean opacity	$\varkappa_R$
KPLK	cm^2/gm	Emission or Planck mean opacity	$\varkappa_P$
LMDAROS	cm	Rosseland mean free path	$\lambda_R = \dfrac{1}{\varkappa_R\rho}$
LMDAPLK	cm	Planck mean free path	$\lambda_P = \dfrac{1}{\varkappa_P\rho}$
TCOOL	sec	Radiative emission cooling time	$t_c = \dfrac{E}{4\sigma\theta^4\varkappa_P}$

DIAPHANOUS DATA   CH2   GENERAL ATOMIC
THETA(EV) =   1.500   SIGMA THETA 4 = 5.194+12

RHO (GM/CM3)	LOG RHO (GM/CM3)	PRESSURE (ERG/CM3)	ENERGY (ERGS/GM)	EION (ERGS/GM)	ZBAR	EGAM
2.340-01	-1.452+00	7.336+10	5.748+11	1.046+11	0.019	1.545
2.211-02	-3.812+00	7.073+09	6.352+11	1.553+11	0.039	1.504
1.620-03	-6.425+00	5.521+08	8.235+11	3.123+11	0.107	1.414
1.226-04	-9.007+00	4.842+07	1.320+12	7.278+11	0.283	1.299
1.202-05	-1.133+01	5.837+06	2.207+12	1.479+12	0.578	1.220
1.638-06	-1.332+01	9.315+05	3.063+12	2.210+12	0.848	1.186
2.639-07	-1.515+01	1.598+05	3.453+12	2.555+12	0.967	1.175
4.324-08	-1.696+01	2.667+04	3.593+12	2.668+12	1.004	1.172
6.334-09	-1.888+01	4.005+03	3.861+12	2.913+12	1.054	1.164
7.229-10	-2.105+01	4.8?7+02	4.669+12	3.653+12	1.201	1.145

RHO (GM/CM3)	LOG RHO (GM/CM3)	KROS (CM2/GM)	KPLK (CM2/GM)	LMDAROS (CM)	LMDAPLK (CM)	TCOOL (SEC)
2.340-01	-1.452+00	1.036+04	3.159+05	4.125-04	1.353-05	8.759-08
2.211-02	-3.812+00	9.107+03	3.056+05	4.966-03	1.480-04	1.001-07
1.620-03	-6.425+00	8.215+03	2.868+05	7.514-02	2.152-03	1.382-07
1.226-04	-9.007+00	5.551+03	2.356+05	1.469+00	3.462-02	2.697-07
1.202-05	-1.133+01	2.448+03	1.429+05	3.398+01	5.820-01	7.434-07
1.638-06	-1.332+01	6.646+02	5.278+04	9.188+02	1.157+01	2.793-06
2.639-07	-1.515+01	1.308+02	1.271+04	2.896+04	2.981+02	1.307-05
4.324-08	-1.696+01	2.545+01	3.048+03	9.088+05	7.589+03	5.675-05
6.334-09	-1.888+01	6.575+00	1.137+03	2.401+07	1.389+05	1.635-04
7.229-10	-2.105+01	1.738+00	4.284+02	7.960+08	3.229+06	5.246-04

DIAPHANOUS DATA   CH2   · GENERAL ATOMIC

THETA(EV) =   2.250   SIGMA THETA 4 =   2.630+13

RHO (GM/CM3)	LOG RHO (GM/CM3)	PRESSURE (ERG/CM3)	ENERGY (ERGS/GM)	EION (ERGS/GM)	ZBAR	EGAM
5.716-02	-2.862+00	3.007+10	1.186+12	3.965+11	0.139	1.444
5.746-03	-5.159+00	3.389+09	1.636+12	7.510+11	0.278	1.361
5.912-04	-7.433+00	4.202+08	2.511+12	1.445+12	0.539	1.283
7.764-05	-9.463+00	6.530+07	3.432+12	2.170+12	0.822	1.245
1.315-05	-1.124+01	1.196+07	3.978+12	2.614+12	0.970	1.229
2.406-06	-1.294+01	2.289+06	4.433+12	3.006+12	1.060	1.215
3.932-07	-1.475+01	3.981+05	5.207+12	3.688+12	1.193	1.194
6.148-08	-1.660+01	6.520+04	5.831+12	4.240+12	1.297	1.182
9.216-09	-1.850+01	9.918+03	6.052+12	4.438+12	1.331	1.178
1.171-09	-2.057+01	1.277+03	6.343+12	4.707+12	1.362	1.172

RHO (GM/CM3)	LOG RHO (GM/CM3)	KROS (CM2/GM)	KPLK (CM2/GM)	LMDAROS (CM)	LMDAPLK (CM)	TCOOL (SEC)
5.716-02	-2.862+00	9.405+04	6.148+05	1.860-04	2.846-05	1.834-08
5.746-03	-5.159+00	6.778+04	5.066+05	2.568-03	3.435-04	3.070-08
5.912-04	-7.433+00	4.062+04	3.249+05	4.164-02	5.207-03	7.348-08
7.764-05	-9.463+00	1.489+04	1.402+05	8.647-01	9.188-02	2.328-07
1.315-05	-1.124+01	4.089+03	4.783+04	1.860+01	1.590+00	7.908-07
2.406-06	-1.294+01	1.111+03	1.945+04	3.742+02	2.137+01	2.167-06
3.932-07	-1.475+01	2.571+02	8.068+03	9.893+03	3.152+02	6.136-06
6.148-08	-1.660+01	4.294+01	2.462+03	3.788+05	6.608+03	2.252-05
9.216-09	-1.850+01	6.350+00	9.219+02	1.709+07	1.177+05	6.242-05
1.171-09	-2.057+01	1.095+00	6.079+02	7.799+08	1.405+06	9.921-05

DIAPHANOUS DATA   CH2   GENERAL ATOMIC

THETA(EV) =   3.400   SIGMA THETA 4 =   1.371+14

RHO (GM/CM3)	LOG RHO (GM/CM3)	PRESSURE (ERG/CM3)	ENERGY (ERGS/GM)	EION (ERGS/GM)	ZBAR	EGAM
3.421-02	-3.375+00	3.420+10	2.481+12	9.809+11	0.433	1.403
4.522-03	-5.399+00	5.221+09	3.537+12	1.805+12	0.655	1.326
6.660-04	-7.314+00	8.780+08	4.581+12	2.603+12	0.890	1.288
1.088-04	-9.126+00	1.586+08	5.536+12	3.349+12	1.089	1.263
1.910-05	-1.087+01	2.986+07	6.446+12	4.102+12	1.240	1.242
3.570-06	-1.254+01	5.797+06	7.068+12	4.632+12	1.328	1.230
6.174-07	-1.430+01	1.039+06	7.860+12	5.337+12	1.411	1.214
9.543-08	-1.616+01	1.699+05	9.302+12	6.631+12	1.552	1.191
1.380-08	-1.810+01	2.553+04	1.035+13	7.574+12	1.651	1.179
1.717-09	-2.018+01	3.265+03	1.130+13	8.452+12	1.725	1.168

RHO (GM/CM3)	LOG RHO (GM/CM3)	KROS (CM2/GM)	KPLK (CM2/GM)	LMDAROS (CM)	LMDAPLK (CM)	TCOOL (SEC)
3.421-02	-3.375+00	2.607+05	5.231+05	1.121-04	5.588-05	8.646-09
4.522-03	-5.399+00	1.804+05	3.062+05	1.226-03	7.222-04	2.106-08
6.660-04	-7.314+00	8.365+04	1.505+05	1.795-02	9.978-03	5.551-08
1.088-04	-9.126+00	2.527+04	7.340+04	3.637-01	1.252-01	1.375-07
1.910-05	-1.087+01	5.163+03	3.584+04	1.014+01	1.460+00	3.280-07
3.570-06	-1.254+01	8.768+02	2.034+04	3.195+02	1.377+01	6.337-07
6.174-07	-1.430+01	1.830+02	1.386+04	8.849+03	1.169+02	1.034-06
9.543-08	-1.616+01	3.448+01	7.869+03	3.039+05	1.332+03	2.155-06
1.380-08	-1.810+01	5.670+00	4.224+03	1.278+07	1.715+04	4.467-06
1.717-09	-2.018+01	1.078+00	2.849+03	5.402+08	2.044+05	7.234-06

DIAPHANOUS DATA   CH2   GENERAL ATOMIC

THETA(EV) =   5.000   SIGMA THETA 4 = 6.412+14

RHO (GM/CM3)	LOG RHO (GM/CM3)	PRESSURE (ERG/CM3)	ENERGY (ERGS/GM)	EION (ERGS/GM)	ZBAR	EGAM
3.566-02	-3.334+00	6.369+10	4.405+12	1.726+12	0.741	1.405
5.680-03	-5.171+00	1.125+10	5.786+12	2.816+12	0.930	1.342
9.345-04	-6.976+00	2.043+09	7.205+12	3.926+12	1.131	1.303
1.600-04	-8.740+00	3.810+08	8.467+12	4.895+12	1.321	1.281
2.865-05	-1.046+01	7.275+07	9.875+12	6.065+12	1.475	1.257
5.238-06	-1.216+01	1.405+07	1.134+13	7.314+12	1.614	1.237
9.010-07	-1.392+01	2.518+06	1.272+13	8.525+12	1.724	1.220
1.412-07	-1.577+01	4.159+05	1.478+13	1.033+13	1.870	1.200
2.062-08	-1.770+01	6.285+04	1.617+13	1.160+13	1.970	1.188
2.647-09	-1.975+01	8.135+03	1.654+13	1.193+13	1.996	1.186

RHO (GM/CM3)	LOG RHO (GM/CM3)	KROS (CM2/GM)	KPLK (CM2/GM)	LMDAROS (CM)	LMDAPLK (CM)	TCOOL (SEC)
3.566-02	-3.334+00	1.855+05	3.234+05	1.511-04	8.670-05	5.310-09
5.680-03	-5.171+00	1.426+05	1.819+05	1.234-03	9.677-04	1.240-08
9.345-04	-6.976+00	6.948+04	1.042+05	1.540-02	1.027-02	2.697-08
1.600-04	-8.740+00	2.088+04	7.259+04	2.993-01	8.609-02	4.547-08
2.865-05	-1.046+01	4.331+03	5.160+04	8.060+00	6.765-01	7.461-08
5.238-06	-1.216+01	8.000+02	3.437+04	2.386+02	5.554+00	1.286-07
9.010-07	-1.392+01	1.508+02	2.287+04	7.357+03	4.852+01	2.168-07
1.412-07	-1.577+01	2.803+01	1.036+04	2.526+05	6.706+02	5.459-07
2.062-08	-1.770+01	4.221+00	2.402+03	1.149+07	2.19+04	2.625-06
2.647-09	-1.975+01	7.221-01	3.396+02	5.232+08	1.113+06	1.898-05

DIAPHANOUS DATA   CH2   GENERAL ATOMIC

THETA(EV) =   7.000   SIGMA THETA 4 = 2.463+15

RHO (GM/CM3)	LOG RHO (GM/CM3)	PRESSURE (ERG/CM3)	ENERGY (ERGS/GM)	EION (ERGS/GM)	ZBAR	EGAM
4.490-02	-3.103+00	1.273+11	6.631+12	2.376+12	0.974	1.428
7.616-03	-4.878+00	2.351+10	8.547+12	3.917+12	1.149	1.361
1.281-03	-6.660+00	4.354+09	1.047+13	5.370+12	1.366	1.325
2.264-04	-8.393+00	8.280+08	1.244+13	6.956+12	1.546	1.294
4.079-05	-1.011+01	1.591+08	1.441+13	8.554+12	1.716	1.271
7.490-06	-1.180+01	3.087+07	1.650+13	1.032+13	1.869	1.25
1.310-06	-1.355+01	5.578+06	1.789+13	1.150+13	1.965	1.238
2.195-07	-1.533+01	9.437+05	1.832+13	1.187+13	1.993	1.235
3.367-08	-1.721+01	1.451+05	1.842+13	1.196+13	1.999	1.234
4.376-09	-1.925+01	1.885+04	1.844+13	1.198+13	2.000	1.234

RHO (GM/CM3)	LOG RHO (GM/CM3)	KROS (CM2/GM)	KPLK (CM2/GM)	LMDAROS (CM)	LMDAPLK (CM)	TCOOL (SEC)
4.490-02	-3.103+00	9.396+04	2.196+05	2.370-04	1.014-04	3.064-09
7.616-03	-4.878+00	8.351+04	1.366+05	1.572-03	9.610-04	6.348-09
1.281-03	-6.660+00	4.855+04	9.713+04	1.608-02	8.038-03	1.094-08
2.264-04	-8.393+00	1.438+04	7.022+04	3.072-01	6.290-02	1.798-08
4.079-05	-1.011+01	3.139+03	4.878+04	7.810+00	5.125-01	2.997-08
7.490-06	-1.180+01	6.223+02	2.342+04	2.146+02	5.702+00	7.152-08
1.310-06	-1.355+01	8.469+01	6.331+03	9.015+03	1.206+02	2.868-07
2.195-07	-1.533+01	1.058+01	1.201+03	4.306+05	3.795+03	1.549-06
3.367-08	-1.721+01	1.614+00	1.899+02	1.839+07	1.564+05	9.845-06
4.376-09	-1.925+01	4.365-01	2.487+01	5.235+08	9.187+06	7.523-05

DIAPHANOUS DATA   CH2   GENERAL ATOMIC
THETA(EV) =   10.000   SIGMA THETA 4 = 1.026+16

RHO (GM/CM3)	LOG RHO (GM/CM3)	PRESSURE (ERG/CM3)	ENERGY (ERGS/GM)	EION (ERGS/GM)	ZBAR	EGAM
6.208-02	-2.779+00	2.807+11	9.853+12	3.070+12	1.230	1.459
1.052-02	-4.554+00	5.225+10	1.261+13	5.163+12	1.420	1.394
1.884-03	-6.275+00	9.997+09	1.527+13	7.304+12	1.587	1.348
3.373-04	-7.994+00	1.919+09	1.790+13	9.371+12	1.772	1.318
6.234-05	-9.683+00	3.732+08	1.993+13	1.095+13	1.917	1.300
1.208-05	-1.132+01	7.384+07	2.081+13	1.163+13	1.979	1.294
2.202-06	-1.303+01	1.354+07	2.109+13	1.187+13	1.996	1.291
3.737-07	-1.480+01	2.300+06	2.118+13	1.194+13	1.999	1.291
5.747-08	-1.667+01	3.538+05	2.120+13	1.197+13	2.000	1.290
7.471-09	-1.871+01	4.591+04	2.121+13	1.198+13	2.000	1.290

RHO (GM/CM3)	LOG RHO (GM/CM3)	KROS (CM2/GM)	KPLK (CM2/GM)	LMDAROS (CM)	LMDAPLK (CM)	TCOOL (SEC)
6.208-02	-2.779+00	3.859+04	1.488+05	4.175-04	1.082-04	1.613-09
1.052-02	-4.554+00	3.494+04	1.004+05	2.720-03	9.467-04	3.061-09
1.884-03	-6.275+00	2.325+04	6.613+04	2.283-02	8.028-03	5.625-09
3.373-04	-7.994+00	8.266+03	3.721+04	3.586-01	7.967-02	1.172-08
6.234-05	-9.683+00	1.530+03	1.365+04	1.048+01	1.175+00	3.557-08
1.208-05	-1.132+01	2.109+02	3.523+03	3.925+02	2.350+01	1.439-07
2.202-06	-1.303+01	2.860+01	7.062+02	1.588+04	6.431+02	7.277-07
3.737-07	-1.480+01	4.366+00	1.237+02	6.129+05	2.164+04	4.172-06
5.747-08	-1.667+01	9.175-01	1.923+01	1.897+07	9.046+05	2.686-05
7.471-09	-1.871+01	3.629-01	2.511+00	3.689+08	5.330+07	2.058-04

DIAPHANOUS DATA   CH2   GENERAL ATOMIC

THETA(EV) =   15.000   SIGMA THETA 4 =   5.194+16

RHO (GM/CM3)	LOG RHO (GM/CM3)	PRESSURE (ERG/CM3)	ENERGY (ERGS/GM)	EION (ERGS/GM)	ZBAR	EGAM
9.543-02	-2.349+00	7.161+11	1.501+13	3.751+12	1.438	1.500
1.679-02	-4.087+00	1.362+11	1.883+13	6.667+12	1.635	1.431
3.053-03	-5.792+00	2.629+10	2.200+13	9.079+12	1.798	1.392
5.745-04	-7.462+00	5.148+09	2.413+13	1.069+13	1.911	1.371
1.117-04	-9.100+00	1.020+09	2.515+13	1.145+13	1.966	1.363
2.204-05	-1.072+01	2.030+08	2.558+13	1.176+13	1.992	1.360
4.040-06	-1.242+01	3.728+07	2.574+13	1.189+13	1.999	1.359
6.863-07	-1.419+01	6.337+06	2.580+13	1.195+13	2.000	1.358
1.056-07	-1.606+01	9.748+05	2.582+13	1.197+13	2.000	1.358
1.372-08	-1.810+01	1.267+05	2.585+13	1.200+13	2.000	1.357

RHO (GM/CM3)	LOG RHO (GM/CM3)	KROS (CM2/GM)	KPLK (CM2/GM)	LMDAROS (CM)	LMDAPLK (CM)	TCOOL (SEC)
9.543-02	-2.349+00	1.091+04	8.170+04	9.607-04	1.283-04	8.842-10
1.679-02	-4.087+00	7.611+03	4.632+04	7.825-03	1.286-03	1.957-09
3.053-03	-5.792+00	3.949+03	2.260+04	8.294-02	1.449-02	4.685-09
5.745-04	-7.462+00	1.260+03	7.548+03	1.381+00	2.306-01	1.539-08
1.117-04	-9.100+00	2.780+02	1.906+03	3.220+01	4.697+00	6.350-08
2.204-05	-1.072+01	5.499+01	4.331+02	8.249+02	1.047+02	2.842-07
4.040-06	-1.242+01	9.783+00	8.388+01	2.530+04	2.951+03	1.477-06
6.863-07	-1.419+01	1.837+00	1.492+01	7.931+05	9.762+04	8.319-06
1.056-07	-1.606+01	5.197-01	2.721+00	1.823+07	3.481+06	4.568-05
1.372-08	-1.810+01	2.755-01	7.739-01	2.645+08	9.416+07	1.608-04

DIAPHANOUS DATA   CH2   GENERAL ATOMIC

THETA(EV) =   22.500   SIGMA THETA 4 =   2.630+17

RHO (GM/CM3)	LOG RHO (GM/CM3)	PRESSURE (ERG/CM3)	ENERGY (ERGS/GM)	EION (ERGS/GM)	ZBAR	EGAM
1.572-01	-1.850+00	1.890+12	2.174+13	3.709+12	1.604	1.553
2.833-02	-3.564+00	3.636+11	2.644+13	7.188+12	1.780	1.485
5.370-03	-5.227+00	7.136+10	2.954+13	9.612+12	1.878	1.450
1.039-03	-6.870+00	1.411+10	3.126+13	1.088+13	1.942	1.435
2.043-04	-8.496+00	2.806+09	3.210+13	1.150+13	1.975	1.428
4.043-05	-1.012+01	5.592+08	3.260+13	1.185+13	1.996	1.424
7.397-06	-1.181+01	1.026+08	3.320+13	1.238+13	2.005	1.418
1.240-06	-1.360+01	1.737+07	3.560+13	1.460+13	2.033	1.393
1.814-07	-1.552+01	2.628+06	4.487+13	2.314+13	2.139	1.323
2.205-08	-1.763+01	3.346+05	5.794+13	3.517+13	2.287	1.262

RHO (GM/CM3)	LOG RHO (GM/CM3)	KROS (CM2/GM)	KPLK (CM2/GM)	LMDAROS (CM)	LMDAPLK (CM)	TCOOL (SEC)
1.572-01	-1.850+00	3.246+03	3.662+04	1.959-03	1.737-04	5.645-10
2.833-02	-3.564+00	1.600+03	1.626+04	2.206-02	2.171-03	1.546-09
5.370-03	-5.227+00	5.328+02	5.382+03	3.495-01	3.460-02	5.219-09
1.039-03	-6.870+00	1.462+02	1.527+03	6.586+00	6.305-01	1.946-08
2.043-04	-8.496+00	3.357+01	4.199+02	1.458+02	1.166+01	7.269-08
4.043-05	-1.012+01	7.816+00	1.632+02	3.164+03	1.515+02	1.899-07
7.397-06	-1.181+01	1.974+00	1.036+02	6.847+04	1.305+03	3.046-07
1.240-06	-1.360+01	7.281-01	8.544+01	1.107+06	9.436+03	3.962-07
1.814-07	-1.552+01	3.792-01	5.661+01	1.454+07	9.739+04	7.536-07
2.205-08	-1.763+01	2.596-01	1.963+01	1.747+08	2.311+06	2.806-06

84

DIAPHANOUS DATA   CH2   GENERAL ATOMIC

THETA(EV) =   34.000   SIGMA THETA 4 =   1.371+18

RHO (GM/CM3)	LOG RHO (GM/CM3)	PRESSURE (ERG/CM3)	ENERGY (ERGS/GM)	EION (ERGS/GM)	ZBAR	EGAM
2.731-01	-1.298+00	5.173+12	3.164+13	3.230+12	1.715	1.599
5.035-02	-2.989+00	1.005+12	3.723+13	7.291+12	1.860	1.536
9.700-03	-4.636+00	1.984+11	4.063+13	9.948+12	1.931	1.503
1.892-03	-6.270+00	3.934+10	4.356+13	1.236+13	1.981	1.477
3.651-04	-7.915+00	7.775+09	4.916+13	1.721+13	2.053	1.433
6.857-05	-9.588+00	1.524+09	6.065+13	2.731+13	2.186	1.366

RHO (GM/CM3)	LOG RHO (GM/CM3)	KROS (CM2/GM)	KPLK (CM2/GM)	LMDAROS (CM)	LMDAPLK (CM)	TCOOL (SEC)
2.731-01	-1.298+00	1.587+03	1.523+04	2.308-03	2.404-04	3.788-10
5.035-02	-2.989+00	5.617+02	6.282+03	3.535-02	3.161-03	1.080-09
9.700-03	-4.636+00	1.722+02	3.116+03	5.986-01	3.308-02	2.377-09
1.892-03	-6.270+00	4.596+01	2.079+03	1.150+01	2.543-01	3.820-09
3.651-04	-7.915+00	1.441+01	1.617+03	1.901+02	1.694+00	5.543-09
6.857-05	-9.588+00	5.226+00	1.029+03	2.790+03	1.417+01	1.075-08

DIAPHANOUS DATA   CH2   GENERAL ATOMIC

THETA(EV) =   50.000   SIGMA THETA 4 =   6.412+18

RHO (GM/CM3)	LOG RHO (GM/CM3)	PRESSURE (ERG/CM3)	ENERGY (ERGS/GM)	EION (ERGS/GM)	ZBAR	EGAM
4.678-01	-7.597-01	1.337+13	4.608+13	3.215+12	1.785	1.620
8.651-02	-2.447+00	2.601+12	5.495+13	9.844+12	1.931	1.547
1.616-02	-4.125+00	5.086+11	6.582+13	1.861+13	2.068	1.478
3.004-03	-5.808+00	9.937+10	8.089+13	3.126+13	2.224	1.409
5.616-04	-7.485+00	1.947+10	9.689+13	4.488+13	2.380	1.358
1.055-04	-9.157+00	3.825+09	1.140+14	5.964+13	2.533	1.318

RHO (GM/CM3)	LOG RHO (GM/CM3)	KROS (CM2/GM)	KPLK (CM2/GM)	LMDAROS (CM)	LMDAPLK (CM)	TCOOL (SEC)
4.678-01	-7.597-01	1.694+03	1.224+04	1.262-03	1.747-04	1.468-10
8.651-02	-2.447+00	5.590+02	8.448+03	2.068-02	1.368-03	2.536-10
1.616-02	-4.125+00	1.932+02	6.414+03	3.203-01	9.649-03	4.001-10
3.004-03	-5.808+00	6.124+01	4.031+03	5.436+00	8.258-02	7.823-10
5.616-04	-7.485+00	1.751+01	2.201+03	1.017+02	8.089-01	1.716-09
1.055-04	-9.157+00	4.801+00	9.266+02	1.974+03	1.023+01	4.797-09

DIAPHANOUS DATA   CH2   GENERAL ATOMIC

THETA(EV) =   70.000   SIGMA THETA 4 =   2.463+19

RHO (GM/CM3)	LOG RHO (GM/CM3)	PRESSURE (ERG/CM3)	ENERGY (ERGS/GM)	EION (ERGS/GM)	ZBAR	EGAM
7.098-01	-3.427-01	3.007+13	7.054+13	6.991+12	1.849	1.601
1.303-01	-2.038+00	5.846+12	8.921+13	2.191+13	2.124	1.503
2.402-02	-3.729+00	1.140+12	1.091+14	3.789+13	2.304	1.435
4.465-03	-5.411+00	2.231+11	1.297+14	5.472+13	2.479	1.385
8.508-04	-7.069+00	4.402+10	1.438+14	6.622+13	2.602	1.360
1.674-04	-8.695+00	8.764+09	1.491+14	7.055+13	2.644	1.351

RHO (GM/CM3)	LOG RHO (GM/CM3)	KROS (CM2/GM)	KPLK (CM2/GM)	LMDAROS (CM)	LMDAPLK (CM)	TCOOL (SEC)
7.098-01	-3.427-01	2.798+03	1.354+04	5.036-04	1.040-04	5.286-11
1.303-01	-2.038+00	1.026+03	9.541+03	7.483-03	8.043-04	9.489-11
2.402-02	-3.729+00	3.027+02	5.824+03	1.375-01	7.148-03	1.901-10
4.465-03	-5.411+00	7.233+01	2.723+03	3.097+00	8.224-02	4.833-10
8.508-04	-7.069+00	1.456+01	8.489+02	8.072+01	1.384+00	1.719-09
1.674-04	-8.695+00	2.771+00	1.959+02	2.156+03	3.048+01	7.721-09

DIAPHANOUS DATA   CH2   GENERAL ATOMIC

THETA(EV) =   100.000   SIGMA THETA 4 =   1.026+20

RHO (GM/CM3)	LOG RHO (GM/CM3)	PRESSURE (ERG/CM3)	ENERGY (ERGS/GM)	EION (ERGS/GM)	ZBAR	EGAM
1.105+00	9.978-02	7.115+13	1.129+14	1.631+13	2.138	1.570
2.035-01	-1.592+00	1.387+13	1.397+14	3.742+13	2.322	1.488
3.760-02	-3.281+00	2.711+12	1.638+14	5.563+13	2.513	1.440
7.243-03	-4.928+00	5.364+11	1.773+14	6.618+13	2.609	1.418
1.430-03	-6.550+00	1.069+11	1.822+14	7.007+13	2.643	1.410
2.846-04	-8.164+00	2.135+10	1.840+14	7.143+13	2.656	1.408

RHO (GM/CM3)	LOG RHO (GM/CM3)	KROS (CM2/GM)	KPLK (CM2/GM)	LMDAROS (CM)	LMDAPLK (CM)	TCOOL (SEC)
1.105+00	9.978-02	3.347+03	1.071+04	2.704-04	8.449-05	2.568-11
2.035-01	-1.592+00	1.340+03	6.121+03	3.668-03	8.030-04	5.561-11
3.760-02	-3.281+00	3.361+02	2.602+03	7.913-02	1.022-02	1.534-10
7.243-03	-4.928+00	5.853+01	7.231+02	2.359+00	1.909-01	5.974-10
1.430-03	-6.550+00	9.215+00	1.855+02	7.587+01	4.224+00	2.682-09
2.846-04	-8.164+00	1.848+00	3.500+01	1.901+03	1.004+02	1.281-08

DIAPHANOUS DATA   CH2   GENERAL ATOMIC

THETA(EV) = 150.000   SIGMA THETA 4 = 5.194+20

RHO (GM/CM3)	LOG RHO (GM/CM3)	PRESSURE (ERG/CM3)	ENERGY (ERGS/GM)	EION (ERGS/GM)	ZBAR	EGAM
1.855+00	6.179-01	1.907+14	1.812+14	2.705+13	2.340	1.567
3.476-01	-1.057+00	3.742+13	2.112+14	4.975+13	2.497	1.510
6.681-02	-2.706+00	7.400+12	2.284+14	6.223+13	2.599	1.485
1.319-02	-4.329+00	1.475+12	2.357+14	6.796+13	2.633	1.474
2.618-03	-5.945+00	2.943+11	2.390+14	7.039+13	2.653	1.470
5.223-04	-7.557+00	5.882+10	2.404+14	7.145+13	2.659	1.468

RHO (GM/CM3)	LOG RHO (GM/CM3)	KROS (CM2/GM)	KPLK (CM2/GM)	LMDAROS (CM)	LMDAPLK (CM)	TCOOL (SEC)
1.855+00	6.179-01	1.021+03	5.042+03	5.278-04	1.069-04	1.730-11
3.476-01	-1.057+00	3.924+02	1.960+03	7.332-03	1.468-03	5.187-11
6.681-02	-2.706+00	1.078+02	5.811+02	1.388-01	2.576-02	1.892-10
1.319-02	-4.329+00	2.308+01	1.375+02	3.286+00	5.517-01	8.253-10
2.618-03	-5.945+00	4.744+00	2.982+01	8.051+01	1.281+01	3.859-09
5.223-04	-7.557+00	1.208+00	6.165+00	1.584+03	3.105+02	1.877-08

89

```
        DIAPHANOUS DATA              CH2        GENERAL ATOMIC
   THETA(EV) =  225.000     SIGMA THETA 4 =  2.630+21

      RHO       LOG RHO   PRESSURE   ENERGY      EION       ZBAR    EGAM
   (GM/CM3)    (GM/CM3)  (ERG/CM3) (ERGS/GM)  (ERGS/GM)

   3.220+00    1.170+00   5.168+14   2.725+14   3.180+13    2.476   1.589
   6.180-01   -4.813-01   1.022+14   2.995+14   5.154+13    2.580   1.552
   1.219-01   -2.105+00   2.035+13   3.132+14   6.270+13    2.617   1.533
   2.410-02   -3.725+00   4.058+12   3.204+14   6.784+13    2.647   1.525
   4.807-03   -5.338+00   8.109+11   3.233+14   7.027+13    2.654   1.522
   9.589-04   -6.950+00   1.621+11   3.249+14   7.138+13    2.661   1.520


      RHO       LOG RHO    KROS      KPLK      LMDAROS    LMDAPLK   TCOOL
   (GM/CM3)    (GM/CM3)  (CM2/GM)  (CM2/GM)     (CM)       (CM)    (SEC)

   3.220+00    1.170+00   1.738+02   1.657+03   1.786-03   1.874-04   1.563-11
   6.180-01   -4.813-01   6.450+01   5.769+02   2.509-02   2.805-03   4.936-11
   1.219-01   -2.105+00   1.553+01   1.350+02   5.283-01   6.076-02   2.205-10
   2.410-02   -3.725+00   4.029+00   3.102+01   1.030+01   1.337+00   9.819-10
   4.807-03   -5.338+00   1.182+00   6.439+00   1.759+02   3.230+01   4.774-09
   9.589-04   -6.950+00   4.939-01   1.323+00   2.111+03   7.883+02   2.335-08
```

90

DIAPHANOUS DATA   CH2   GENERAL ATOMIC

THETA(EV) =   340.000   SIGMA THETA 4 =   1.371+22

RHO (GM/CM3)	LOG RHO (GM/CM3)	PRESSURE (ERG/CM3)	ENERGY (ERGS/GM)	EION (ERGS/GM)	ZBAR	EGAM
5.731+00	1.746+00	1.433+15	4.038+14	2.872+13	2.584	1.619
1.132+00	1.242-01	2.857+14	4.290+14	5.053+13	2.616	1.588
2.244-01	-1.494+00	5.699+13	4.428+14	6.185+13	2.640	1.574
4.474-02	-3.107+00	1.139+13	4.492+14	6.740+13	2.648	1.567
8.918-03	-4.720+00	2.275+12	4.528+14	7.005+13	2.657	1.564
1.781-03	-6.330+00	4.549+11	4.544+14	7.128+13	2.661	1.562

RHO (GM/CM3)	LOG RHO (GM/CM3)	KROS (CM2/GM)	KPLK (CM2/GM)	LMDAROS (CM)	LMDAPLK (CM)	TCOOL (SEC)
5.731+00	1.746+00	4.031+01	3.803+02	4.328-03	4.587-04	1.936-11
1.132+00	1.242-01	1.149+01	1.561+02	7.688-02	5.656-03	5.009-11
2.244-01	-1.494+00	3.116+00	3.593+01	1.430+00	1.240-C1	2.247-10
4.474-02	-3.107+00	1.010+00	7.587+00	2.213+01	2.946+00	1.080-09
8.918-03	-4.720+00	4.688-01	1.581+00	2.392+02	7.094+01	5.223-09
1.781-03	-6.330+00	3.033-01	3.218-01	1.851+03	1.744+03	2.575-08

DIAPHANOUS DATA   CH2   GENERAL ATOMIC

THETA(EV) = 500.000   SIGMA THETA 4 = 6.412+22

RHO (GM/CM3)	LOG RHO (GM/CM3)	PRESSURE (ERG/CM3)	ENERGY (ERGS/GM)	EION (ERGS/GM)	ZBAR	EGAM
1.013+01	2.315+00	3.749+15	5.796+14	2.439+13	2.608	1.639
2.012+00	6.992-01	7.484+14	6.061+14	4.820+13	2.625	1.614
3.997-01	-9.169-01	1.494+14	6.214+14	6.073+13	2.643	1.601
7.952-02	-2.532+00	2.984+13	6.298+14	6.688+13	2.657	1.596
1.590-02	-4.142+00	5.967+12	6.329+14	6.981+13	2.659	1.593
3.175-03	-5.752+00	1.193+12	6.348+14	7.117+13	2.662	1.592

RHO (GM/CM3)	LOG RHO (GM/CM3)	KROS (CM2/GM)	KPLK (CM2/GM)	LMDAROS (CM)	LMDAPLK (CM)	TCOOL (SEC)
1.013+01	2.315+00	1.092+01	1.996+02	9.039-03	4.946-04	1.132-11
2.012+00	6.992-01	3.196+00	4.964+01	1.555-01	1.001-02	4.761-11
3.997-01	-9.169-01	1.068+00	1.103+01	2.341+00	2.269-01	2.197-10
7.952-02	-2.532+00	4.887-01	2.320+00	2.573+01	5.420+00	1.058-09
1.590-02	-4.142+00	3.117-01	4.735-01	2.018+02	1.328+02	5.210-09
3.175-03	-5.752+00	2.532-01	9.614-02	1.244+03	3.276+03	2.574-08

DIAPHANOUS DATA   CH2   GENERAL ATOMIC

THETA(EV) = 700.000   SIGMA THETA 4 = 2.463+23

RHO (GM/CM3)	LOG RHO (GM/CM3)	PRESSURE (ERG/CM3)	ENERGY (ERGS/GM)	EION (ERGS/GM)	ZBAR	EGAM
1.671+01	2.816+00	8.685+15	7.985+14	1.888+13	2.618	1.651
3.328+00	1.202+00	1.735+15	8.277+14	4.570+13	2.629	1.630
6.618-01	-4.128-01	3.464+14	8.448+14	5.957+13	2.644	1.620
1.317-01	-2.027+00	6.919+13	8.545+14	6.635+13	2.658	1.615

RHO (GM/CM3)	LOG RHO (GM/CM3)	KROS (CM2/GM)	KPLK (CM2/GM)	LMDAROS (CM)	LMDAPLK (CM)	TCOOL (SEC)
1.671+01	2.816+00	4.208+00	8.175+01	1.422-02	7.321-04	9.913-12
3.328+00	1.202+00	1.383+00	1.937+01	2.172-01	1.551-02	4.337-11
6.618-01	-4.128-01	5.795-01	4.139+00	2.607+00	3.651-01	2.071-10
1.317-01	-2.027+00	3.439-01	8.750-01	2.208+01	8.678+00	9.910-10

DIAPHANOUS DATA   CH2   GENERAL ATOMIC
THETA(EV) = 1000.000   SIGMA THETA 4 = 1.026+24

RHO (GM/CM3)	LOG RHO (GM/CM3)	PRESSURE (ERG/CM3)	ENERGY (ERGS/GM)	EION (ERGS/GM)	ZBAR	EGAM
2.846+01	3.348+00	2.117+16	1.128+15	1.226+13	2.625	1.659
5.675+00	1.736+00	4.230+15	1.161+15	4.268+13	2.633	1.642
1.130+00	1.220-01	2.450+14	1.180+15	5.817+13	2.645	1.634
2.249-01	-1.492+00	1.688+14	1.192+15	6.574+13	2.658	1.630

RHO (GM/CM3)	LOG RHO (GM/CM3)	KROS (CM2/GM)	KPLK (CM2/GM)	LMDAROS (CM)	LMDAPLK (CM)	TCOOL (SEC)
2.846+01	3.348+00	1.862+00	3.309+01	1.887-02	1.062-03	8.307-12
5.675+00	1.736+00	7.231-01	7.361+00	2.437-01	2.394-02	3.843-11
1.130+00	1.220-01	3.904-01	1.579+00	2.268+00	5.606-01	1.821-10
2.249-01	-1.492+00	2.812-01	3.307-01	1.582+01	1.345+01	8.781-10

DIAPHANOUS DATA   CH2   GENERAL ATOMIC

THETA(EV) = 2250.000   SIGMA THETA 4 =   2.630+25

RHO (GM/CM3)	LOG RHO (GM/CM3)	PRESSURE (ERG/CM3)	ENERGY (ERGS/GM)	EION (ERGS/GM)	ZBAR	EGAM
9.580+01	4.562+00	1.606+17	2.509+15	6.202+12	2.632	1.668
1.897+01	2.943+00	3.204+16	2.568+15	3.441+13	2.659	1.658
3.796+00	1.334+00	6.409+15	2.587+15	5.452+13	2.657	1.653
7.588-01	-2.760-01	1.282+15	2.598+15	6.416+13	2.658	1.650

RHO (GM/CM3)	LOG RHO (GM/CM3)	KROS (CM2/GM)	KPLK (CM2/GM)	LMDAROS (CM)	LMDAPLK (CM)	TCOOL (SEC)
9.580+01	4.562+00	5.619-01	4.843+00	1.858-02	2.156-03	4.926-12
1.897+01	2.943+00	3.378-01	1.019+00	1.561-01	5.175-02	2.397-11
3.796+00	1.334+00	2.633-01	2.139-01	1.000+00	1.232+00	1.150-10
7.588-01	-2.760-01	2.380-01	4.347-02	5.537+00	3.031+01	5.681-10